Tectonics

RESEARCH ARTICLE
10.1029/2021TC007027

Protracted Thermal Evolution of a Migmatitic Terrane as Revealed by Multiple Geochronometers From the Retro-Arc of the Early Paleozoic Famatinian Orogen in NW Argentina

Pablo Farias[1], Roberto F. Weinberg[1], Alfonso Sola[2], and Melanie Finch[1,3]

[1]School of Earth, Atmosphere and Environment, Monash University, Clayton, VIC, Australia, [2]IBIGEO-CONICET Instituto de Bio y Geociencias del NOA, Consejo Nacional de Investigaciones Científicas y Técnicas – Universidad Nacional de Salta, Salta, Argentina, [3]Now at Department of Earth and Environmental Sciences, James Cook University, Townsville, QLD, Australia

Abstract U-Pb dates of zircon, monazite, and titanite combined with trace element composition, allows characterization of the thermal evolution of the migmatitic Agua del Sapo complex. This complex comprises Al-rich and Ca-rich metasedimentary rocks with a detrital zircon maximum depositional age of 550 Ma. The rocks record two consecutive early Paleozoic orogenies. During subduction associated with the 550–510 Ma Pampean orogeny, the complex was in the fore-arc region and was intruded by 550–520 Ma granites indicative of anomalous heating possibly related to ridge subduction. During the subsequent 500–440 Ma Famatinian orogeny, the arc migrated trenchwards and the region became part of a retro-arc that underwent melting at upper-amphibolite facies. This event was recorded differently by each of the accessory phases. Detrital zircon cores were overgrown by rare Famatinian rims that range from 500 to 420 Ma, while monazite records only Famatinian dates with a growth peak at ~457 Ma that extends to 410 Ma, possibly due to coupled dissolution-precipitation. Published titanite dates define a 120 Myr thermal history, starting at ~500 Ma with temperatures of ~750°C ± 25°C, ending at 380 Ma and ~700°C ± 25°C. Cooling was accompanied by a decrease in titanite light rare earth element contents in response to increased abundance of allanite/epidote. Thus, the complementary time-compositional record of the accessory phases reveals continued high heat flow, associated with deformation, to 380 Ma. This prolonged event blurs the boundary between the Famatinian and the subsequent Achalian/Chanic orogenies and extends the Silurian Rinconada tectonic phase of the Famatinian orogeny to the east into the Eastern Sierras Pampeanas.

Key Points:

- Zircon U-Pb dates reveal a Pampean-age granite intruded into the fore-arc of the Pampean orogeny, overprinted by Famatinian-age metamorphism
- Titanite records a 120 Myr-long Famatinian metamorphism with slow cooling from 750°C to 700°C, accompanied by a decrease in light rare earth element contents
- This prolonged high-T thermal and deformation history blurs the boundary between the Famatinian and the subsequent Achalian/Chanic orogen

Supporting Information:

Supporting Information may be found in the online version of this article.

Correspondence to:

R. F. Weinberg,
Roberto.Weinberg@monash.edu

Citation:

Farias, P., Weinberg, R. F., Sola, A., & Finch, M. (2023). Protracted thermal evolution of a migmatitic terrane as revealed by multiple geochronometers from the retro-arc of the early Paleozoic Famatinian orogen in NW Argentina. *Tectonics*, *42*, e2021TC007027. https://doi.org/10.1029/2021TC007027

Received 20 AUG 2021
Accepted 11 FEB 2023

Author Contributions:

Conceptualization: Roberto F. Weinberg
Data curation: Pablo Farias
Formal analysis: Pablo Farias
Funding acquisition: Roberto F. Weinberg
Investigation: Pablo Farias, Roberto F. Weinberg, Alfonso Sola, Melanie Finch
Project Administration: Roberto F. Weinberg
Supervision: Roberto F. Weinberg

1. Introduction

There is increasing evidence that the middle and lower orogenic crusts can remain at temperatures close to or above their solidus for tens of million years. This is the case for the Early Paleozoic Famatinian orogen, the subject here (Finch et al., 2017, 2021; Wolfram et al., 2019); for the Brasiliano-Panafrican Araçuaí orogen in southeastern Brazil (Cavalcante et al., 2018; Fossen & Cavalcante, 2017; Vauchez et al., 2019) or southern India, where suprasolidus temperatures lasted for at least 35 Myr and probably much longer (Johnson et al., 2015; Taylor et al., 2014); and also Central Iberia, where Variscan anatexis lasted 55 Myr (Montero et al., 2004). In Arctic Norway, monazite showed large spread of dates and homogeneous compositions indicating that the region could have remained at elevated temperatures of >600°C for over ca. 200 Ma, at relatively static conditions, for most of the Neoproterozoic (Gasser et al., 2015). However, for rocks of the same complex, Kirkland et al. (2016) found that the date spreads were due to monazite susceptibility to fluid alteration, which leave the framework of the crystal intact, but purge its radiogenic-Pb.

Prolonged anatexis raises questions about the nature of the heat source capable of generating and maintaining these conditions for over tens of millions of years. Bea (2012) discussed the three main possible heat sources and concluded that a combination of moderately high mantle heat flow and a thick fertile crust with moderate heat production, common to "volcanic and back-arc areas of subduction zones, is ideal to produce copious granite magmatism." For the retro-arc of the Famatinian orogen, a continental crust with relatively high contents of heat-producing elements would not be enough to sustain the metamorphic conditions and would require increased mantle heat flux (Wolfram et al., 2019). The nature of anatectic events, including duration, heat flow, melt productivity and thermal buffering, controls the nature of migmatites and of granitic rocks, and hence heat and mass transfer within continents (Brown, 2010, 2013) that in turn control the architecture of orogens and ultimately the architecture of continents.

Writing – original draft: Pablo Farias
Writing – review & editing: Roberto F. Weinberg

Another key question is the impact of melting on the lithospheric response to orogenic stresses. In particular, the nature and duration of the metamorphic conditions in the overriding plates of subduction zones are fundamental for determining the rheological evolution of the crust and hence the nature of deformation and crustal thicknesses during mountain building. Finally, knowledge of the thermal structure and evolution of orogens is a key natural constraint to test predictions from numerical models. As an example of such constraints, the debated channel flow models of southward extrusion of hot middle crust in the Tibetan orogen, requires long-lived anatexis (Beaumont et al., 2001; Faccenda et al., 2008) that is not always recorded by the exposed migmatites (Finch et al., 2014).

In this paper, we detail the tectono-thermal evolution of the retro-arc of the Paleozoic Famatinian orogen in NW Argentina, where migmatites record anatexis that lasted continuously or intermittently for at least 60 Myr, from 500 to 440 Ma (Finch et al., 2017, 2021; Wolfram et al., 2019). This conclusion was based in part on U-Pb dating of zircon and monazite from rocks of the Tolombon complex in the hanging wall of a major thrust in the Sierra de Quilmes. One monazite sample from the Agua del Sapo complex in the footwall, yielded younger ages between 440 and 420 Ma (Finch et al., 2017), suggesting that high temperatures may have continued below the shear zone long after cooling of the hanging wall. This was confirmed by Farias et al. (2020) who investigated titanite from footwall samples and concluded that this retro-arc region "remained above 700°C for 120 Myr between 500 and 380 Ma" some 60 Myr longer than the hanging wall. In this paper, we expand on these finding by investigating the complementary temporal and thermal record of zircon, monazite and titanite of several samples from the footwall. Our aim is to confirm, detail and better constrain the tectono-thermal evolution of the retro-arc.

Each of these accessory minerals has different closure temperatures below which their U-Pb isotopic system start working as geochronometers (Braun et al., 2006; Kirkland et al., 2017; Rollinson, 1995). The effective closure temperature (T_c) depends on factors like diffusivity of a particular element (D), grain shape and size, and cooling rate (Dodson, 1973). Zircon and monazite closure temperatures are >900°C (Cherniak & Pyle, 2008; Cherniak & Watson, 2001; Gardés et al., 2007; Kelsey et al., 2008; Lee et al., 1997), and titanite seems to vary widely from 450°C to 500°C (Mattinson, 1978) to over 825°C (Gao et al., 2012), but most recent studies agree that its closure temperature is above 660°C, possibly >700°C (Kohn, 2017). Further to that, each of these geochronometers responds differently to complex geological histories leading to zoned accessory phases that reflect changes not only in P-T but also deformation and fluid flow, that can trigger regrowth, dissolution-reprecipitation, recrystallization or diffusion.

In melt-bearing rocks, such as investigated here, the stability of these accessory minerals, and hence their U-Pb record, largely depends on their solubility in the melt phase. This is in turn dependent on melt temperature and composition (e.g., Kelsey et al., 2008). In migmatites, these phases can dissolve and regrow as conditions fluctuate, leading to variable records (e.g., Finch et al., 2021). Another important process is coupled dissolution-precipitation, particularly in monazite. In rocks of the Tolombon complex, the U-Pb record of monazite has been affected by this process, which caused a spread of dates and a decoupling between dates and the trace element zonation of the grains (Weinberg et al., 2020). Improvements of analytical tools, such as the *laser ablation split stream* (LASS-ICP-MS), allow us to investigate the U-Pb date and trace element composition of the same spot in a single zone within the grain. The integration of such data for zircon, monazite, and titanite is a powerful tracer of petrogenetic processes (Rubatto, 2002; Scibiorski et al., 2019; Taylor et al., 2016; Whitehouse & Platt, 2003).

In this paper, we bring together new zircon and monazite dates with the previously published titanite results by Farias et al. (2020). By integrating the results from these different chronometers with titanite trace element chemistry and thermodynamic modeling, we conclude that the Famatinian orogeny is marked by long-lived metamorphism at temperatures between 750°C and 700°C, from the start of the Famatinian orogeny at 500 to 380 Ma. Each of the three accessory phases responded differently to the tectono-metamorphic evolution, with titanite providing the most extensive record, with little sign of recrystallization.

2. Geological Background

2.1. Sierras Pampeanas and the Paleozoic Orogenies

The Sierra de Quilmes, where the Agua del Sapo complex is exposed (Rossi & Toselli, 1976), is one of the mountain ranges that form the Sierras Pampeanas, a series of north-south trending mountain ranges in NW Argentina, uplifted in the Andean foreland (Figure 1). These mountains now expose rocks that were part of a Paleozoic

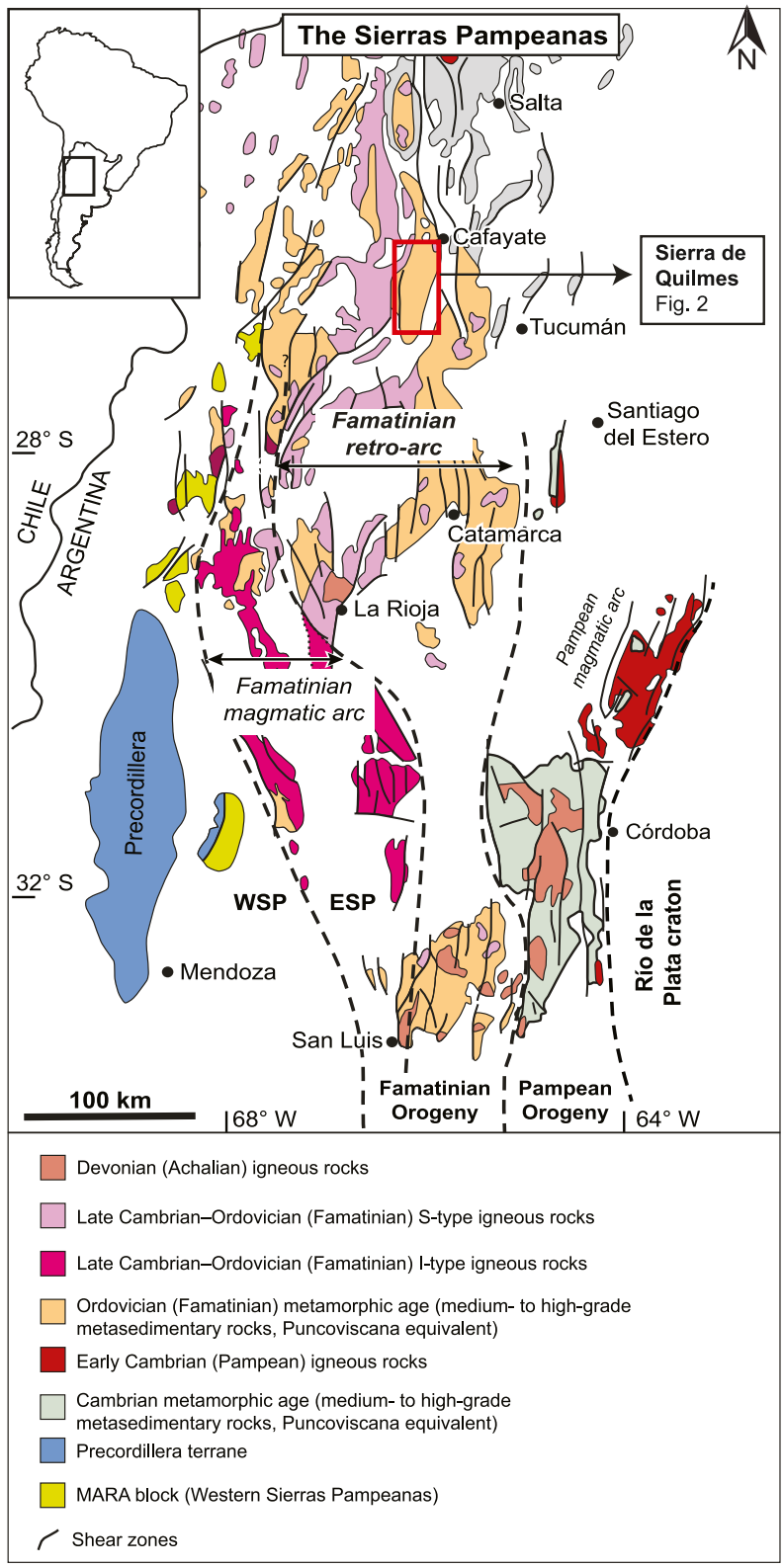

Figure 1. Map of the Sierras Pampeanas and location of the Sierra de Quilmes (red rectangle). The Pampean magmatic arc is in the east, against the tectonic contact with the Río de la Plata craton, and the Famatinian arc is to the west. WSP and ESP refer to the Western and Eastern Sierras Pampeanas, respectively.

accretionary margin along the Western Gondwana supercontinent margin, part of the Terra Australis orogen (Cawood, 2005). This region underwent three early Paleozoic orogenies: the Pampean (ca. 540–520 Ma), the Famatinian (ca. 500–440 Ma) and the Achalian or Chanic (ca. 400–350 Ma) orogenies (see review in Weinberg et al., 2018). These orogenies were controlled by subduction and accretion of different Laurentian terranes (Aceñolaza et al., 2002; Astini, 1998; Escayola et al., 2011; Omarini et al., 1999; Ramos et al., 1986, 2010; Rapela, Pankhurst, Saavedra, et al., 1998, Rapela et al., 2016). The amalgamation of these exotic terranes to the accretionary margin formed a composite block known as the Western Sierras Pampeanas (WSP; Figure 1). In between the WSP in the west and the Rio de la Plata craton in the east, lies the Eastern Sierras Pampeanas (ESP). The ESP includes the Sierra de Quilmes and are composed largely by metasedimentary rocks derived from turbidites, and igneous rocks derived from arc magmatism and from the melting of the turbidites (Adams et al., 2011). These turbidites were deposited initially in the passive margin of Western Gondwana between ca. 670 and 550 Ma (Adams et al., 2011; Omarini et al., 1999; Rapela, Pankhurst, Saavedra, et al., 1998), with sediments sourced from the craton. Subsequently, this margin developed into the active accretionary margin of the Pampean orogeny, with renewed turbidite deposition in the fore-arc region with sediments sourced from the Pampean magmatic arc between 550 and 520 Ma. Collectively these rocks are known as the Puncoviscana sequence (Weinberg et al., 2018).

The Pampean magmatic arc crops out discontinuously from the Sierra de Córdoba in the south to the Cordillera Oriental in the north of Argentina (Figure 1) (e.g., Dahlquist et al., 2016). Schwartz et al. (2008) divided the Pampean arc into a calc-alkaline belt in the east and a peraluminous high-temperature, medium to high-pressure migmatitic belt in the west. The Pampean orogeny and its arc magmatism ended with the arrival of a Laurentian continental ribbon, known as MARA (Casquet et al., 2005; Rapela et al., 2007, 2016), that clogged the subduction zone at ca. 520-510 Ma (Martino, 2003; Otamendi et al., 2004; Pankhurst et al., 2000; Rapela et al., 1998a; Schwartz et al., 2008). Subduction restarted soon after the end of the Pampean orogeny, giving rise to the Famatinian arc, some 200 km trenchwards from the Pampean arc (e.g., Otamendi et al., 2020). Renewed subduction was first associated with an extensional phase leading to deposition of Ordovician marine sedimentary rocks in the back-arc. This was followed by shortening and mountain building (Weinberg et al., 2018). The Famatinian orogenic cycle refers to this entire tectono-magmatic cycle.

2.1.1. Famatinian Orogenic Cycle and the Oclóyic Phase

The Famatinian orogenic cycle was a subduction-related, Andean-type continental orogeny initiated at ca. 505–500 Ma, as suggested by U-Pb zircon ages in S-type magmatic rocks of its retro-arc region (Bahlburg et al., 2016; Wolfram et al., 2017). This orogeny resulted in a north-south striking, 1,600 km-long magmatic arc coupled to the east with an intensely deformed and metamorphosed retro-arc overprinting the previous Pampean fore-arc. The retro-arc melted profusely forming a belt of S-type granites known as the Eastern Eruptive Belt. Arc magmatism occurred between ca. 490 and ca. 440 Ma with a peak at 470 Ma (Bahlburg et al., 2016; Ducea et al., 2010, 2017; Mulcahy et al., 2014; Pankhurst et al., 1998, 2000; Rapela et al., 2018; Wolfram et al., 2017) coeval with peak metamorphism and extensive anatexis in the retro-arc (Büttner et al., 2005; Casquet, Alasino, et al., 2021; Finch et al., 2017; Lucassen et al., 2011; Radice et al., 2021; Sola et al., 2013, 2017).

The tectonic regime in the Famatinian retro-arc changed from extensional to compressional when the Laurentian-derived micro-continent known as the Precordillera terrane approached and docked on the western margin of Gondwana (Astini, 1998; Astini et al., 1995; Otamendi et al., 2020). This initiated the Oclóyic phase of deformation (Turner, 1975) that led to mountain building and the inversion of Ordovician marine basins. This event is marked by regional unconformities (Astini & Dávila, 2004; Bahlburg & Hervé, 1997) and is associated with kilometer-wide mylonitic-ultramylonitic thrust zones (Finch et al., 2015; Larrovere et al., 2016; Rapela et al., 1998b; Semenov & Weinberg, 2017; Semenov et al., 2019). The Famatinian cycle finished at around 440-435 Ma when magmatism and anatexis waned (Bahlburg et al., 2016; Büttner, 2009; Büttner et al., 2005; Mulcahy et al., 2014; Wolfram et al., 2017).

2.2. Geology of the Sierra de Quilmes: Three Metamorphic Complexes

The Sierra de Quilmes is a mountain range in the north of the ESP province. It extends ~130 km north-south and is ~30 km wide (Figure 2). The protolith of its metasedimentary and igneous rocks is the Puncoviscana sequence (Büttner et al., 2005; Rapela, 1976a; Toselli et al., 1978). The Sierra de Quilmes exposes the mid-crustal section

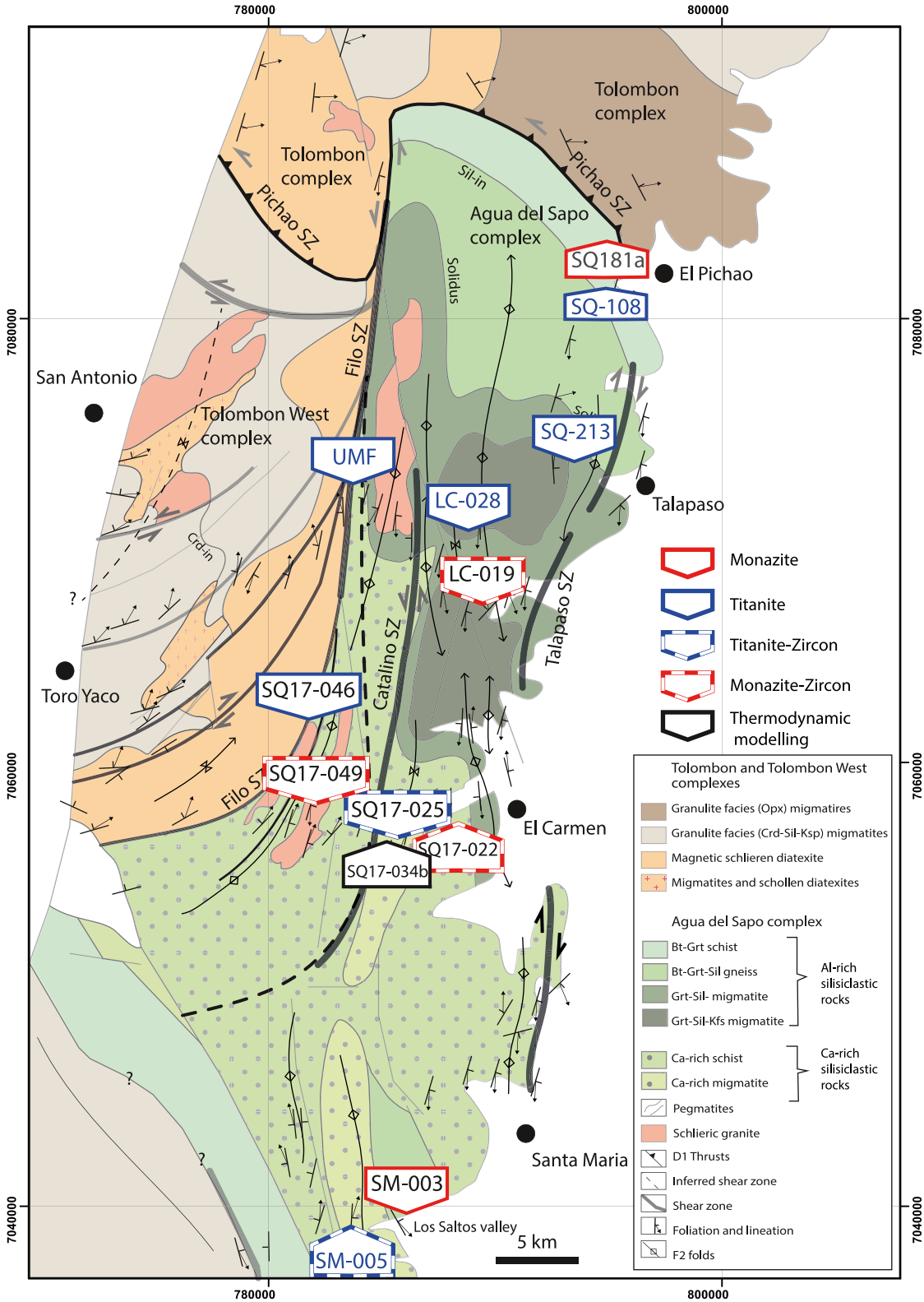

Figure 2. Simplified geological map of part of the Sierra de Quilmes with sample location and the minerals analyzed in each sample. Also shown is the location of the sample used for thermodynamic modelling (Figure 4). Sample coordinates are listed in Table 2.

of the Famatinian retro-arc, dominated by high-temperature and low-pressure (HT-LP) metamorphism (Büttner et al., 2005; Rapela, 1976a, 1976b; Wolfram et al., 2017). These conditions were established during the early, extensional phase of the Famatinian orogenic cycle (Büttner, 2009). The Oclóyic phase gave rise to intense thrusting and folding, and wide (ultra)mylonitic shear zones (Finch et al., 2015).

The Sierra de Quilmes is composed of three metamorphic complexes intruded by peraluminous igneous rocks (Farias et al., 2020): the Tolombon complex in the north, the Tolombon West complex in the southwest, and the Agua del Sapo complex in the southeast (Figure 2). These complexes are separated by two major, interconnected amphibolite facies shear zones with a greenschist facies overprint. The Filo Shear Zone strikes roughly north-south and separates the Agua del Sapo complex in the east from the Tolombon West complex in the west. The Filo Shear Zone has sinistral kinematics with a sub-horizontal stretching lineation (Farias et al., 2020) and links northwards to the curved but generally NE-dipping Pichao Shear Zone, which is an oblique west-verging thrust (Finch et al., 2015). The two interconnected shear zones form the Pichao-Filo Thrust System. This system juxtaposes different rock sheets within a thrust duplex system: the Tolombon was thrusted over the Tolombon West complex, and both were thrusted over the Agua del Sapo complex.

In this paper, we will refer to the Tolombon and Tolombon West complexes, as the hanging wall complexes. They comprise Al-rich siliciclastic turbidites metamorphosed to migmatites during the Famatinian orogenic cycle (Finch et al., 2017). Peak metamorphic conditions in the Tolombon complex reached granulite facies conditions at ~6 kbar and 800°C, determined in the orthopyroxene zone (Büttner et al., 2005; Finch et al., 2017). Extensive migmatization was accompanied by the formation of S-type leucogranitic plutons (Wolfram et al., 2017). The Tolombon West complex is lithologically similar, but lacks the orthopyroxene zone, being dominated by garnet-cordierite-sillimanite migmatites, similar to those in the eastern part Tolombon complex where Büttner et al. (2005) established metamorphic conditions of 650°C–750°C and <5 kbar. The thrust separating them has a top-to-west syn-anatectic kinematics (Farias et al., 2020).

2.2.1. Agua Del Sapo Complex

This complex, in the footwall of the Pichao-Filo Thrust System, was first described by Rossi and Toselli (1976). The metamorphic grade increases from north to south, from Bt-Grt-Sil amphibolite facies rocks (mineral abbreviations after Kretz, 1983), lacking evidence of anatexis, to migmatites with a Grt-Sil-Kfs mineral paragenesis toward the south (Figure 2). In the northern part of the complex, the rocks are also derived from the Al-rich siliciclastic turbiditic sequence with cordierite and sillimanite. However, some 20 km to the south, these rocks transition to Ca-rich siliciclastic metasedimentary rocks (Figure 2), with primary layering and graded bedding (Toselli et al., 1978). They are dominantly hornblende-bearing migmatites with the Ca-rich paragenesis of hornblende-plagioclase-biotite-quartz-titanite-epidote-allanite and occasionally clinopyroxene and scapolite. The structural architecture of the Agua del Sapo complex is different from the hanging wall complexes (see Farias et al., 2020). Here, the top-to-west thrusts that dominate the hanging wall (Finch et al., 2017) are overprinted by a pervasive top-to-south shearing with a strong sub-horizontal, north-south trending stretching lineation parallel to constrictional sheath folds and upright open folds (the D2 of Farias et al., 2020). The structures are interpreted as recording a non-coaxial constriction with horizontal stretching and south-verging thrusting (Farias et al., 2020).

2.3. Previous Geochronology

Most of the dating in the Sierra de Quilmes has focused on the Tolombon complex (Büttner et al., 2005; Finch et al., 2017; Lucassen et al., 2000; Weinberg et al., 2020; Wolfram et al., 2019), with only two dated samples from the north end of the Agua del Sapo complex (Finch et al., 2017). Results reveal Famatinian ages of magma crystallization and metamorphism for both hanging wall and footwall (Table 1). Wolfram et al. (2019) and Finch et al. (2021) dated zircons from diatexites and leucocratic granites of the Tolombon complex by means of LA-ICP-MS. The results show a wide date spread between 505 and 440 Ma, suggesting protracted high-temperature conditions and multiple anatectic events (Wolfram et al., 2019). Lucassen et al. (2000) estimated the timing of high-grade metamorphism to be ca. 440 Ma based on the Sm/Nd age of calc-silicate rocks in granulite facies rocks of the Tolombon complex. This is significantly younger than the 477 ± 11 Ma Sm/Nd age based on a garnet aplite whole-rock isochron of Büttner et al. (2005). These authors obtained U-Pb TIMS monazite ages of ca. 470 Ma. However, the total dissolution of grains used in this technique could potentially produce mixed ages. Finch et al. (2017) reported two monazite U-Pb SHRIMP age populations at 484.8 ± 2.3

Table 1
Summary of Geochronological Data From Previous Studies in the Sierra de Quilmes (Büttner et al., 2005; Finch et al., 2017; Lucassen et al., 2000; Weinberg et al., 2020)

	Zircon (U-Pb) (Ma)	Monazite (U-Pb) (Ma)[a]	Titanite (U-Pb) (Ma)	Muscovite (Ar-Ar)(Ma)[a]	Sm/Nd (Ma)[a]	Rb/Sr (Ma)[a]
Tolombon complex	ca. 505[b]	500–450[c]	459–468[d]	442 ± 11[e]	442 ± 9[f]	450 ± 7[g]
	ca. 490[b]	473 ± 4[h]		408 ± 7[i]	477 ± 11[j]	416 ± 6[k]
	ca. 475–465[b]	468 ± 2[h]				
	ca. 460[b]	484.8 ± 2.3[l]				
	ca. 450–445[b]	470.7 ± 2.2[l]				
Agua del Sapo complex		463.6 ± 2.2[m]				
		484.6 ± 2.6[m]				
		420.8 ± 1.8[n]				
		435.2 ± 1.9[n]				

[a]All uncertainties are 2σ. [b]Five different age peaks were determined between ca. 500 and ca. 445 Ma with the most intense peaks in bold (LA-ICP-MS)(Wolfram et al., 2019). [c]LASS (Weinberg et al., 2020). [d]Calc-silicate in migmatite near Cafayate town (TIMS) (Büttner et al., 2005). [e]Large muscovite grains (Büttner et al., 2005). [f]Isochron (Grt-Pl-WR) in granulite facies calc-silicate rock (Lucassen et al., 2000). [g]Retrograde muscovite from migmatite (Büttner et al., 2005). [h]Bt-Grt-Crd migmatite (TIMS) (Büttner et al., 2005). [i]Small muscovite grains in shear zone (Büttner et al., 2005). [j]Isochron (Grt-Ap-WR) in garnet aplite (Büttner et al., 2005). [k]Fine-grained syn-kinematic muscovite (Büttner et al., 2005). [l]Pichao Shear Zone (SHRIMP) (Finch et al., 2017). [m]Schist at base of Pichao Shear Zone (SHRIMP) (Finch et al., 2017). [n]Schist at the immediate footwall of the Pichao Shear Zone (SHRIMP) (Finch et al., 2017).

and 470.7 ± 2.2 Ma from sheared migmatites of the Pichao Shear Zone. Later, Weinberg et al. (2020) obtained U-Pb LASS monazite dates of migmatites that spread between 500 and 440 Ma, a similar range to the zircon U-Pb dates of the same rocks. However, investigating the relationship between dates and well-defined core-rim zonation, they found that monazite showed no core-rim systematics, and argued that U-Pb dates were decoupled from the mineral chemistry responsible for the zonation. They concluded that this likely reflected coupled dissolution-precipitation processes. The Ar-Ar age of muscovite from pegmatites, with closure temperatures of ~450°C–400°C, yielded ages of 442 ± 11 Ma for coarse grains and 408 ± 7 Ma for fine-grained muscovite in small shear zones (Büttner et al., 2005).

For the Agua del Sapo complex, Finch et al. (2017) reported monazite U-Pb SHRIMP dates from a mylonitic Bt-Grt schist sample collected right at the base of the Pichao Shear Zone. This sample yielded monazite dates of ca. 470 Ma, which are comparable with the monazite dates of the hanging wall Tolombon complex. However, a schist sampled ~1 km to the south, records unusually young monazite, with dates between 435 and 420 Ma. Finch et al. (2017) argued that the young ages could be the result of heating of the amphibolite-facies rocks in the footwall following the overthrusting of the granulite-facies Tolombon complex.

The most extensive dating work of rocks of the Agua del Sapo complex was the U-Pb dating of titanites by Farias et al. (2020). They found widely variable ranges of dates. Their seven samples collectively range from ~500 to 380 Ma, but date ranges vary significantly from sample to sample, indicating different titanite growth times. Here, we compare the U-Pb dates and chemistry of zircon, titanite and monazite of a variety of samples to better understand the tectono-thermal evolution of the footwall complex. The complex is particularly well-suited for this comparison because rocks typically have pairs of datable accessory phases: the Al-rich siliciclastic rocks generally have Zrn + Mnz whereas the Ca-rich ones have Zrn + Ttn. We analyzed these minerals by means of LASS-ICP-MS (laser-ablation split-stream inductively coupled plasma mass spectrometry) and LA-ICP-MS for two of the monazite samples (see Table 2). The new data are integrated with available data to interpret the history of these rocks and critically assess the response of each of these geochronometers to the long-lasting metamorphism.

3. Analytical Methods

3.1. LA-ICP-MS and LASS-ICP-MS

Samples were crushed and milled and an aliquot was separated for geochemical analysis and the rest for mineral separation. The latter was sieved and the fraction finer than <355 μm was washed, and the heaviest fraction

Table 2
Summary of Samples Divided Into Al-Rich and Ca-Rich Siliciclastic Rocks

Sample	*Rock seq.*	*Rock type*	*Notes*	*Mineral paragenesis*	*Zrn*	*Mnz*	*Ttn*	*mounted grains (M) or in situ*
SM-003	Al-rich	Metatexite	Weakly sheared	Qtz-Bt-Pl-Kfs-Sil-Grt		LA		M
E785028								
N7038928								
LC-019		Metatexite	In lithon	Qtz-Bt-Pl-Kfs-Grt-Sil-Ms-Tur	LA	LA		M
E789541								
N7066524								
SQ17-022		Leucosome	In lithon	Qtz-Pl-Kfs-Bt-Ms	LASS	LASS		M
E787387								
N7057776								
SQ17-049		Schlieric granite		Qtz-Kfs-Pl-Ms-Bt-Grt- Sil	LASS	LASS		M
E781540								
N7056763								
SQ-181a		Grt-Ms schist		Bt-Ms-Qtz-Pl-Kfs-Grt		*SHRIMP*		M
E796885								
N7077289								
UMF	Ca-rich[a]	Mylonite	Fine-grained	Qtz-Pl-Bt-Hbl-Kfs			LASS	In situ
E780400								
N7050032								
SQ17-025		Hbl-metatexite	Sheared	Qtz-Pl-Bt-Hbl-Kfs	LASS		LASS	M
E786461								
N7057063								
SQ-213		Hbl-schist	Sheared	Bt-Qtz-Pl-Hbl-Kfs			LASS	In situ
E794870								
N7072826								
SQ-108		Hbl-schist	Footwall of PSZ	Bt-Qtz-Pl-Hbl-Kfs			LASS	In situ
E779004								
N7090438								
SQ17-046c		Amphibolite	Sheared FSZ	Hbl-Pl-Qtz-Kfs			LASS	M
E780632								
N7057375								
LC-028		Hbl-metatexite	Weakly sheared	Qtz-Pl-Bt-Kfs-Hbl-Cpx			LASS	In situ
E787767								
N7069006								
SM-005		Hbl-metatexite		Qtz-Pl-Bt-Kfs-Hbl-Scp	LASS		LASS	In situ
E784026								
N7039176								
SQ-039		Calc-silicate nodule	From Tolombon Complex	Qtz-Pl-Bt-Kfs-Hbl			LASS	In situ
E781711								
N7056642								

Note. Sample SQ-181a is from Finch et al. (2017). LA stands for LA-ICP-MS, LASS for LASS-ICP-MS. Coordinates given below each sample in italics are in UTM zone 19.

[a]All samples from the Ca-rich siliciclastic rocks have Ep-Aln-Ap-Ttn as accessory phases except for amphibolite sample SQ17-046c that lack Ep-Aln.

was separated by panning. Heavy minerals were concentrated using conventional magnetic and heavy liquid separation techniques. The epoxy mounts were polished, and the minerals photographed under reflected light in an optic microscope, followed by backscattered electrons (BSE) images at the Center for Electron Microscopy at Monash University using an MCEM JEOL 7001F scanning electron microscope. Zircon was imaged using cathodo-luminescence (CL) on the Philips (FEI) XL30 ESEM TMP electron microscope with a Gatan CL detector at the scanning electron microscope facility at Melbourne University. Five out of seven titanite samples were analyzed in-situ by LASS-ICP-MS. The selected thin sections were polished before BSE imaging. The two titanite separates analyzed were from samples SQ17-025 (Hbl-metatexite) and SQ17-046c (amphibolite) (see Table 2).

The U-Pb zircon, monazite and titanite dating was carried out at the School of Earth, Atmosphere and Environment, Monash University, by means of LA-ICP-MS and LA-ICP-MS in a split stream mode (LASS-ICP-MS). The first two samples (Table 2) were analyzed by LA-ICP-MS where U-Pb and trace elements were analyzed separately using a Thermo ICAPTQ triple quadrupole Inductively Coupled Plasma Mass Spectrometer (ICP-MS) coupled with an ASI Resolution 193 nm excimer laser equipped with a dual volume Laurin Technic S155 ablation cell. For the rest of the samples, the LASS-ICP-MS was used. This allowed us to obtain U-Pb and trace elements from the same spot. The minerals were analyzed using the ASI Resolution 193 nm excimer laser that splits the ablated material in two with one stream directed to the Thermo ICAPTQ triple quadrupole ICP-MS for U-Pb ages, and the other is directed to a Thermo ICAPQ quadrupole ICP-MS where rare earth and selected trace elements were analyzed.

The minerals were sampled in a He atmosphere with a He flow of 550 mL/min and the laser operating at a repetition rate of 10 Hz and a 25 μm spot size. The laser energy used for zircon and titanite was approximately 4 Jcm^{-2} and for monazite 6 Jcm^{-2}. Each analysis began with 20 s measurement of the gas background, followed by 15 s with the laser switched on. The ablated material was split into two equal amounts using a Y junction placed just downstream of the ablation cell.

For the U-Pb dates, the following masses were analyzed: ^{202}Hg, ^{204}Pb, ^{206}Pb, ^{207}Pb, ^{208}Pb, ^{232}Th, and ^{238}U. Dwell time for ^{202}Hg, ^{204}Pb was 30 ms, for ^{206}Pb 40 ms, for ^{207}Pb 70 ms, for ^{208}Pb 20 ms and for ^{232}Th and ^{238}U 10 ms. For the trace elements and some major elements, different masses were analyzed depending on the mineral. For zircon ^{29}Si, ^{47}Ti, ^{49}Ti, ^{89}Y, ^{91}Zr, ^{93}Nb, ^{139}La, ^{140}Ce, ^{141}Pr, ^{146}Nd, ^{147}Sm, ^{153}Eu, ^{157}Gd, ^{159}Tb, ^{163}Dy, ^{165}Ho, ^{166}Er, ^{169}Tm, ^{172}Yb, ^{175}Lu, ^{181}Ta. For titanite, ^{29}Si, ^{44}Ca, ^{88}Sr, ^{89}Y, ^{91}Zr, ^{93}Nb, ^{139}La, ^{140}Ce, ^{141}Pr, ^{146}Nd, ^{147}Sm, ^{153}Eu, ^{157}Gd, ^{159}Tb, ^{163}Dy, ^{165}Ho, ^{166}Er, ^{169}Tm, ^{172}Yb, ^{175}Lu, ^{177}Hf, ^{178}Hf, ^{181}Ta. For monazite ^{31}P, ^{43}Ca, ^{88}Sr, ^{89}Y, ^{91}Zr, ^{93}Nb, ^{139}La, ^{140}Ce, ^{141}Pr, ^{146}Nd, ^{147}Sm, ^{153}Eu, ^{157}Gd, ^{159}Tb, ^{163}Dy, ^{165}Ho, ^{166}Er, ^{169}Tm, ^{172}Yb, ^{175}Lu, ^{181}Ta.

For U-Pb, raw data was reduced using the Iolite 3.6 software (Paton et al., 2010, 2011). Dating, instrumental mass bias, drift, and downhole fractionation were corrected by analyzing different standard materials every half hour throughout the analytical session. For zircon, the Plešovice standard (Sláma et al., 2008) was used as the primary calibration standard, and GJ-1 zircon (Jackson et al., 2004) and Temora 1 zircon (Black et al., 2003) were analyzed as unknowns, or secondary standards, for quality control purposes. For monazite, MAdel (Payne et al., 2008) was used as the primary standard and 44,069 (Aleinikoff et al., 2006) as a secondary standard. Analyses more than 10% discordant were not considered (data available in Table S1). Monazite and zircon were not corrected for common lead. For monazite ratios, the external 2SE uncertainty of 2% from Richter et al. (2019) was used.

For the trace elements, the raw data was reduced using the Iolite 3.6 software and quantitative results were obtained using the NIST610 glass as the primary external standard and using the stoichiometric content of Si in zircon and titanite. The NIST612 glass, USGS standard BHVO 2G and BCR 2G were analyzed throughout the analytical session to check for precision and accuracy of the results. Around 1% of the analysis were discarded during data reduction due to blurred or unclear ICP-MS signal or large error bars. Therefore, some dates are not coupled with trace elements, and vice-versa. U-Pb dating results and trace elements for zircon and monazite as well as validation reference material data are provided in Tables S1 to S3.

3.2. Whole-Rock Geochemistry

Samples were selected for geochemical analysis in order to characterize the nature of the Ca-rich siliciclastic metasedimentary rocks and to carry out thermodynamic modeling. These samples were milled using a

tungsten-carbide grinder. Major element analyses were conducted at the Australian Research Council Center of Excellence in Ore Deposits (CODES), University of Tasmania, Australia, on a Panalytical Axios Advanced 4.0 kW X-Ray Fluorescence (XRF) Spectrometer. Trace element analyses were obtained at the School of Earth Atmosphere and Environment, Monash University, Victoria, Australia, using ICP-MS analyses after conventional acid sample digestion.

At CODES, samples were prepared in 32 mm fusion discs at 1,100°C in 5% Au/95% Pt crucibles, 0.500 g sample, 4.500 g 12–22 Flux (Lithium Tetraborate-Metaborate mix) and 0.0606 g LiNO3 for silicates. Platinum/5% gold molds were used for cooling. Corrections for mass absorption were calculated using PANalytical Super-Q software with its Classic calibration model and alpha coefficients. In-house inter-element corrections were also applied. Pure element oxide mixes in pure silica, along with International and Tasmanian reference rocks were used. Numerous checks of reference rocks and pure silica blanks were run with each program.

At Monash University, trace element analysis was carried out using a Thermo iCAPQ-c, quadrupole ICP-MS. Sample solutions were produced from roughly 50 mg of sample powder, which were then put into sealed Teflon high pressure vessels with a mixture of HF-HNO_3-HCl and placed in the oven at 170°C for approximately 72 hr. After drying, the samples were put back into solution using 2% HNO_3 before analysis with the mass spectrometer. ICP-MS count rates were externally standardized by means of calibration curves based on the in-house basalt standard BNB. Results are listed in Table S5.

3.3. Mineral Chemistry by Electron Microprobe

In order to constrain P-T conditions through thermodynamic modeling, mineral chemistry was obtained at the University of Melbourne by means of electron microprobe (EMP) using a Cameca SX50 EMP with four vertical wavelength dispersive spectrometers (WDS). The electron beam used an accelerating voltage of 15 kV, beam current of 35 nA, and a spot size of 10 μm to minimize migration of volatile elements. Counting times for all elements were 20 s peak and 10 s on two backgrounds on either side of the peak position. Polished thin sections were carbon-coated by carbon vacuum evaporation to 250 Å. The data reduction software used was SAMx with an integrated matrix correction software program PAP (Pouchou & Pichoir, 1991). Mineral structural formula calculations were based on Deer et al. (1992).

3.4. Thermodynamic Modeling

In order to determine peak P-T conditions for the migmatites in the Agua del Sapo complex, we constructed a P-T pseudosection based on the bulk geochemistry of one migmatite sample and constrained the P-T field using the composition for garnet and biotite. The software used for calculating the phase diagram was THERMOCALC v. 3.33 (Powell et al., 1998 and (2009 upgrade)) and the internally consistent thermodynamic data set 5.5, ds55 (Holland & Powell, 1998, 2003). The pseudosections were calculated in the system MnO-Na_2O-CaO-K_2O-FeO-MgO-Al_2O_3-SiO_2-H_2O-TiO_2-O (MnNCKFMASHTO). The amount of water in the model was the amount required to saturate the system at the solidus. In pelites, iron should be mostly Fe^{2+}, but a small proportion of Fe^{3+} is typically present, so we added 0.2 Fe_2O_3, which was subtracted from FeO total. This was added by varying O, as is standard for calculations in THERMOCALC.

The activity-composition models used were as follows: melt from White et al. (2007), cordierite and staurolite from a combination of Mahar et al. (1997) and Holland and Powell (1998), garnet, ilmenite and biotite from White et al. (2005), orthopyroxene from White et al. (2002), muscovite from Coggon and Holland (2002), and plagioclase and K-feldspar from Holland and Powell (2003). Notations used are: almandine = Fe/(Ca + Fe + Mg + Mn), grossular = Ca/(Ca + Fe + Mg + Mn), spessartine = Mn/(Ca + Fe + Mg + Mn), pyrope = Mg/(Ca + Fe + Mg + Mn), X_{Fe} = Fe/(Fe + Mg).

4. Results

4.1. Petrography

Table 2 lists sample coordinates, mineral assemblages, accessory minerals dated and the method used for dating. Figure 2 shows their location on the geological map. Eleven samples were investigated plus sample SQ-181a

dated by Finch et al. (2017) with dates between 440 and 410 Ma. The Al-rich siliciclastic rocks and their melting products are represented by one schist (SQ-181a) (Finch et al., 2017), two metatexite migmatites (SM-003, LC-019), a leucosome (SQ17-022), and a schlieric granite (SQ17-049). Sample SQ-181a is a sheared Grt-Ms schist (Figure 3a) located ~5 km from the Pichao Shear Zone. It has Tur + Ap + Mnz + Zrn as accessory phases. Zircon is typically included in Bt, and Mnz is found as inclusions commonly in Ms but also in Tur. Garnet porphyroblasts are partially retrogressed to Bt + Chl at their edges, and Bt is partially retrogressed to Chl. The two metatexite samples (SM-003, LC-019) have Tur + Ap + Mnz + Zrn as accessory phases. K-feldspar forms large 0.5–1 cm poikiloblasts with rounded inclusions of Qtz and Bt, and fibrolite typically forms ~1 cm "nests" that define crenulations (Figure 3b). Zircon is included in Ms and Bt with pleochroic haloes, but is also found outside them. Monazite is found at contacts between Bt and either Ms or Qtz. The leucosome sample SQ17-022 is a weakly deformed Bt-Ms granite with Qtz with undulose extinction, Pl with poorly developed lamellar twinning and Kfs with patches of tartan twinning. Zircon is found outside and inside Bt, where it forms pleochroic haloes. Monazite is found as inclusions in Bt or at its contact with felsic minerals. The schlieric granite sample (SQ17-049) is part of the Filo granite, an array of igneous bodies that crop out along the western flank of the complex. This weakly foliated granite is elongated north-south, extending for at least 5 km (Figure 2), concordant with the country-rock foliation. This is a Bt + Ms + Grt + Sil granite with Mnz + Zrn and rare Ap as accessory phases. This granite has aligned Bt-Grt-rich schlieren and sometimes 1 cm-long phenocrysts of Kfs with abundant inclusions of Bt and rounded Qtz, similar to those in the migmatites. The Ca-rich siliciclastic rocks are represented by two schist samples (SQ-108 and SQ-213) from within the Al-rich siliciclastic package in the north part of the complex (Figure 2), and three metatexites (SQ17-025, LC-028, SM-005), one amphibolite (SQ17-046c), and one mylonite (UMF) from the Filo Shear Zone, all from the region dominated by Ca-rich rocks in the southern half of Figure 2. All these rocks have Qtz + Hbl + Bt + Kfs + Pl + Ms ± Cal with Ap + Ttn + Ep + Aln + Ilm as accessory phases (Figure 3c). Meionite (Ca-rich scapolite) is present in sample SM-005 as isolated subhedral grains, and Cpx is found in sample LC-028, typically in contact with Hbl and Cal. Titanite in sample SQ17-025 has Ilm cores (Figure 3d). Allanite, light rare earth element (LREE)-rich Ep and Ep form core-mantle-rim textures in all rocks (Figure 3e) except the amphibolite (SQ17-046c), and Zrn is typically inside Bt or Qtz (Figure 3f).

4.2. Thermodynamic Modeling

In order to constrain peak metamorphic conditions, a pseudosection was calculated based on the bulk geochemistry and mineral composition of sample SQ17-034b, a Grt-Sil-Kfs migmatite (Figure 4). This sample is an Al-rich siliciclastic rock that represents the core of the high-grade migmatites of the Agua del Sapo complex. It was the only sample modeled where the mineralogy was in equilibrium with the bulk rock. The other samples, not included here, were out of equilibrium presumably because of magma gain and loss. The results show that the metamorphic peak mineral assemblage Bt + Grt + Kfs + Sil + Pl + Ilm + Liq is stable across a wide range of temperatures (~675°C–775°C), and pressures (4 to >7.5 kbar). Plagioclase in this rock ranges from An 21 to 30, whereas Bt has X_{Fe} between 0.47 and 0.52, and Grt grossular ranges from 0% to 3.5% and almandine from 70% to 74%. The X_{Fe} isopleths for biotite narrow the temperature range to between 710°C and 740°C, while grossular composition of Grt rims constrains the pressure to between 5.5 and 6 kbar (Figure 4). The Grt is zoned with grossular (Ca-Al garnet) and almandine (Fe garnet) components increasing from core to rim, and pyrope (Mg garnet) and spessartine (Mn garnet) decreasing from core to rim, suggestive of prograde growth. Mineral geochemistry details are provided in Table S6.

4.3. Geochronology and Mineral Chemistry

4.3.1. Zircon

All zircon geochronological and chemistry data are presented in Tables S1 and S2, including analytical results for reference materials. Zircons from five samples were investigated (Table 2, sample location in Figure 2), including one from the Filo schlieric granite (SQ17-049), two from migmatites from the Al-rich siliciclastic group (SQ17-022 and LC-019) and two from the Ca-rich siliciclastic group (SQ17-025 and SM-005). Most grains have detrital zircon (DZ) cores (Figure 5). These are rounded or anhedral with younger rims of variable thickness, morphology and CL texture. The interface between DZ cores and rims typically have a thin bright CL fringe and signs of resorption (Figure 5). CL images of the rims are usually featureless, but can also have oscillatory textures, or fuzzy sector zoning (Figure 5).

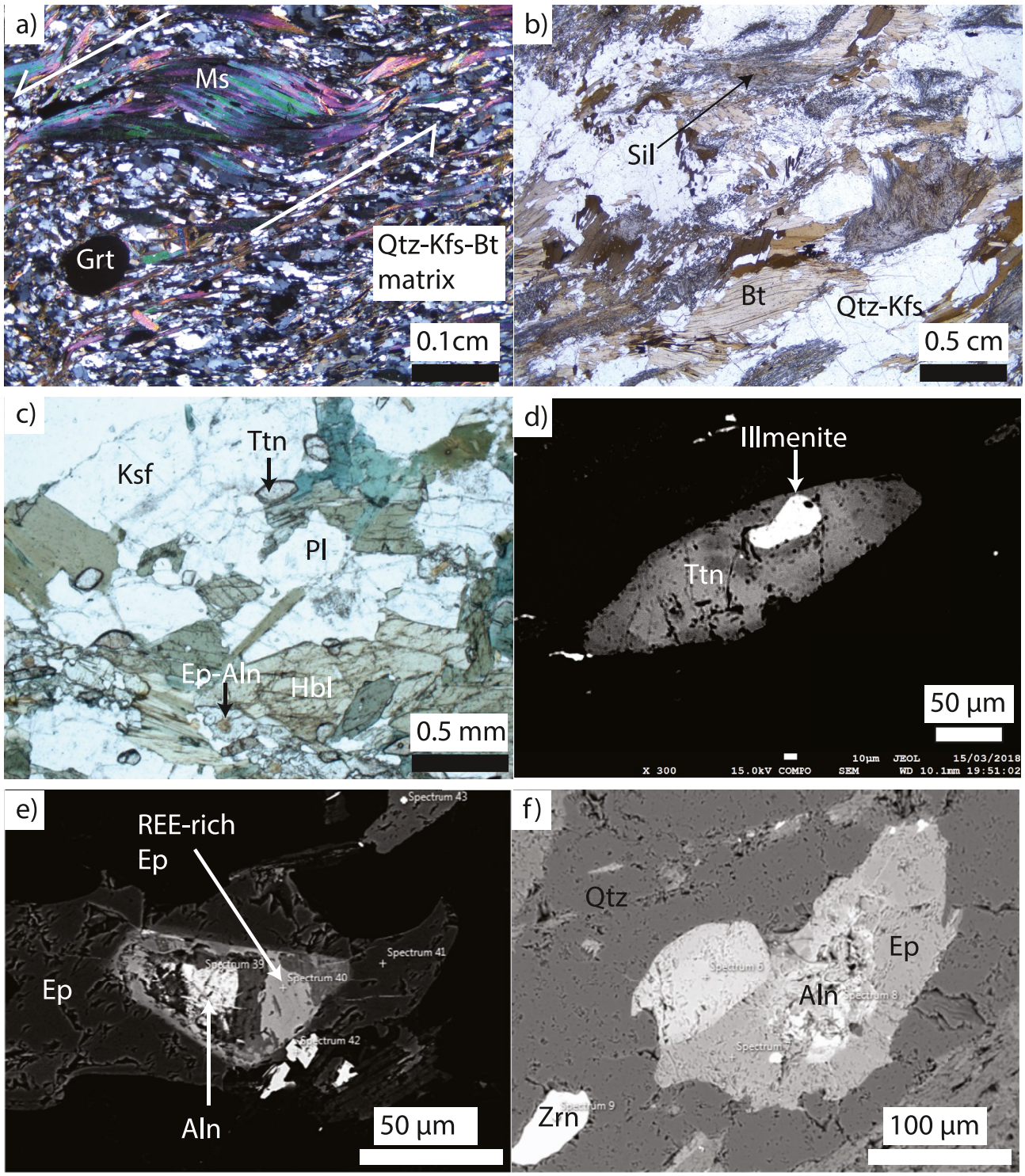

Figure 3. Photomicrographs and SEM images of textures in Al-rich siliciclastic rocks (a, b), and Ca-rich siliciclastic rocks (c–f). (a) Grt-Ms schist SQ-181a (cross-polarized light, XPL) of. (b) Metatexite with abundant Sil (plane-polarized light, PPL). (c) Hornblende-rich rock with Ep + Aln + Ttn (PPL). (d) Titanite with Ilm core. (e) Allanite core, light rare earth element (LREE)-rich Ep mantle, and Ep rim texture. (f) Same as (e), but lacking LREE-rich Ep mantle. Note Zrn grain included in Qtz.

4.3.1.1. Migmatites: Detrital Zircon (DZ) and Famatinian Rims

Detrital zircon dates from migmatite samples cluster in two groups: a broad one ranging from 550 to 690 Ma, and another from 920 to 1,000 Ma with a number of smaller peaks in between (Figure 6). These rocks lack zircon

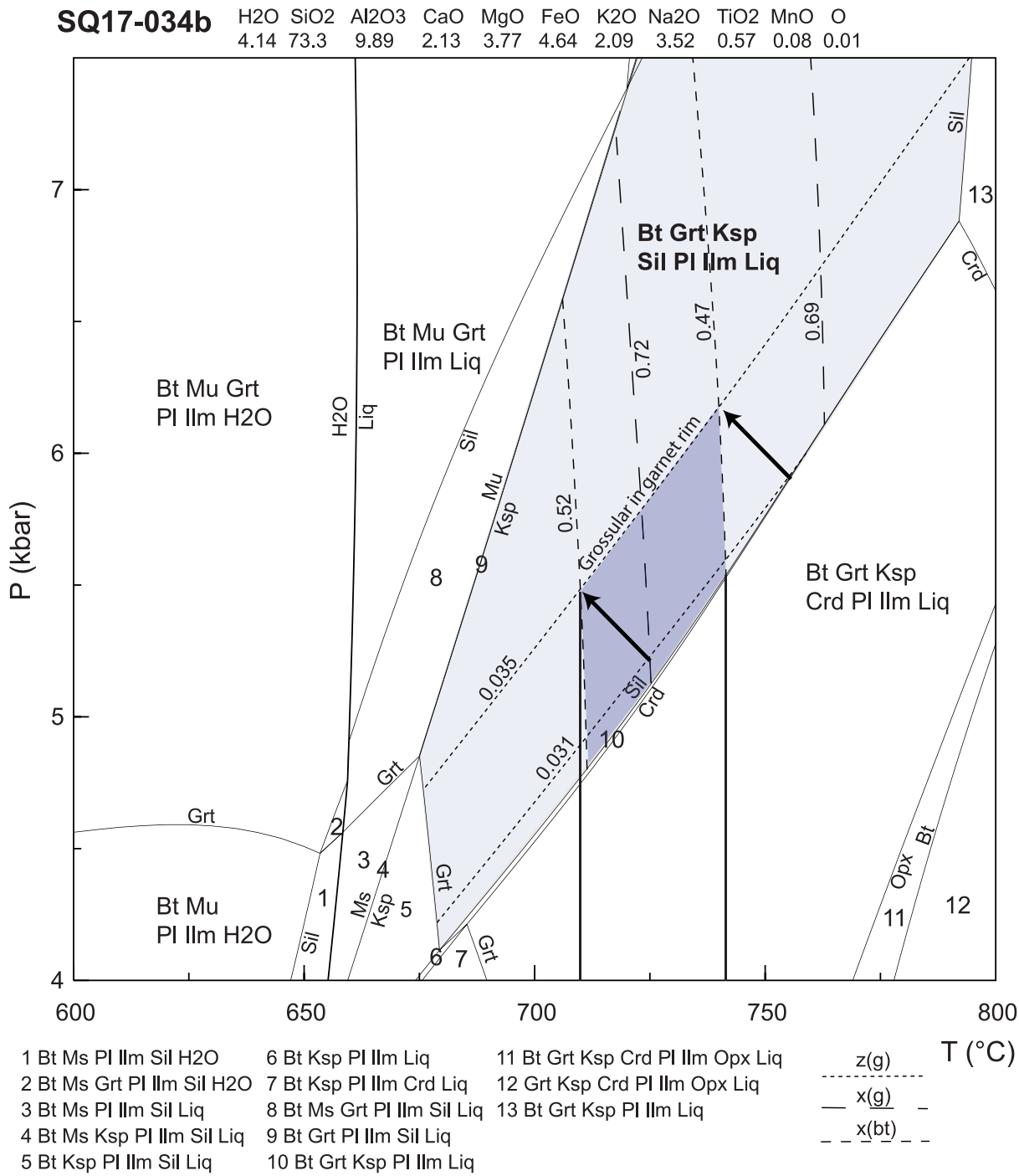

Figure 4. MnO-Na_2O-CaO-K_2O-FeO-MgO-Al_2O_3-SiO_2-H_2O-TiO_2-O (MnNCKFMASHTO) pressure-temperature pseudosection for sample SQ17-034b (coordinates E0783704 N7056799, UTM zone 19). The recalculated whole-rock chemical composition is given above the figure. The stable paragenesis is Bt-Grt-Ksp-Sil-Pl-Ilm + Liq (light gray zone). Isopleths constrain the temperature to 710°C–740°C, and pressure to between 4.5 and 6 kbar. For biotite, x(bt) = Fe/(Fe + Mg) values between 0.47 and 0.52 limit the T field, which overlaps with the average value for almandine in the Grt (0.72 isopleth). Garnet grossular content, z(g), constrains the pressure field. Grossular reaches a maximum value in garnet rims of 0.035 or 3.5%. Garnet almandine content, x(g), varies between 0.70 and 0.74. Black arrows represent the trend of grossular values from mantle to rim.

cores with dates between 550 and 510 Ma belonging to the Pampean orogeny. These were only found in the Filo schlieric granite sample (SQ17-049) where they are occasionally accompanied by thin Famatinian-age rims (Figure 6e).

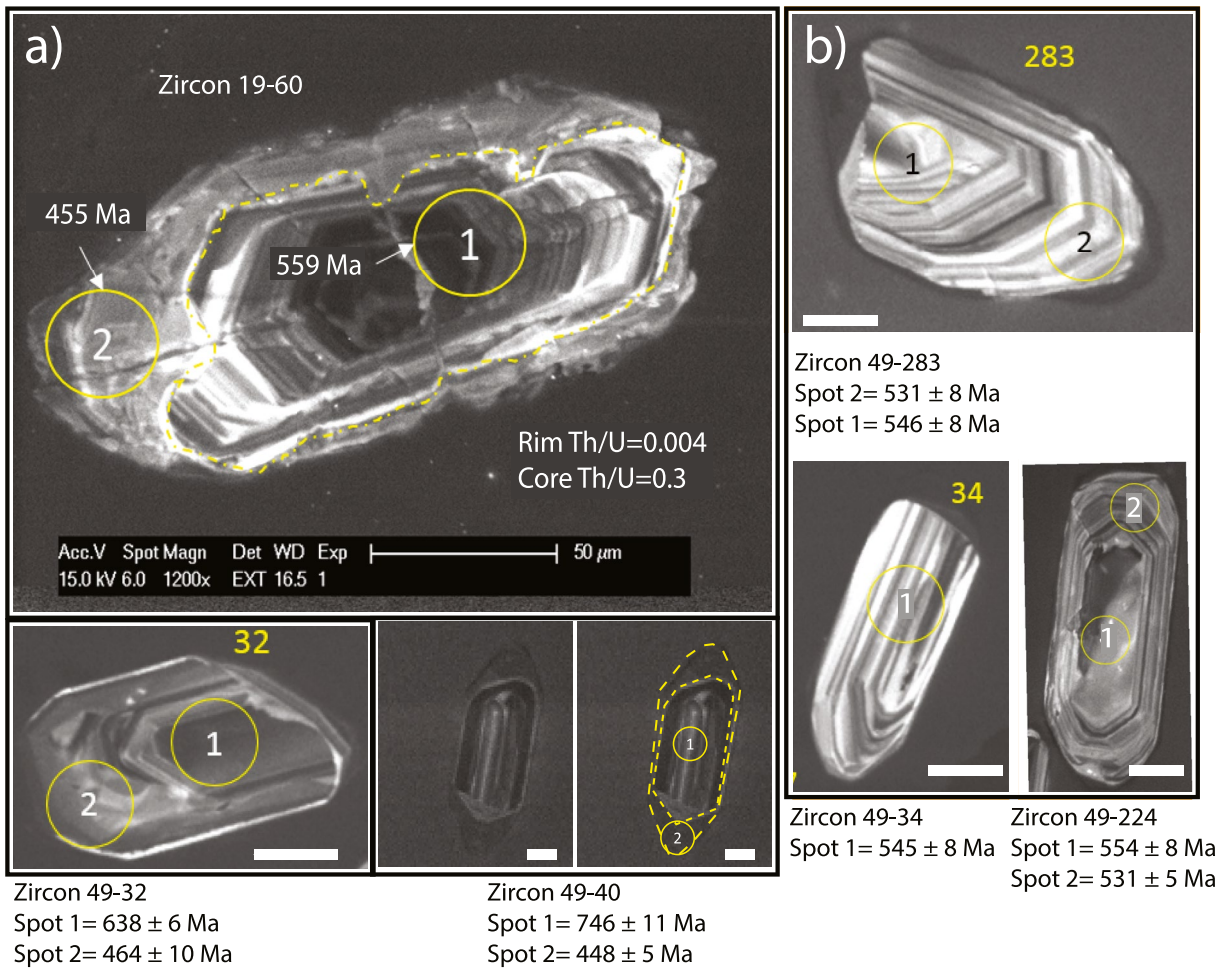

Figure 5. (a) Typical cathodo-luminescence (CL) image of core-rim texture in zircon (large image from sample LC-019). The dissolution front of the detrital zircon (DZ) core is marked by a bright CL line a few µm wide that truncates the internal zonation, indicated by the discontinuous yellow line. The rim has a diffuse irregular zonation and low Th/U ratios. Smaller images below show other examples of zircon rims on DZ from the Filo granite sample SQ17-049. (b) Oscillatory textures in igneous zircon from sample SQ17-049. Yellow numbers correspond to zircon spot number and full zircon labels list first the last two digits of the sample number (e.g., 49 for sample SQ17-049) followed by the zircon spot number given in Table S1.

Three of the migmatitic samples yielded only a small number of Famatinian dates in zircon rims (LC-019, SQ17-022, and SM-005), the fourth sample, SQ17-025, did not have rims wide enough for the laser spot. The Famatinian dates scatter between 498 and 424 Ma (Figure 7). These dates are typically from zircon rims and occasionally from cores (LC-019). The rims are not considered metamict, as the CL textures do not indicate radiation damage and their U content is less than 1,000 ppm (Table S1).

4.3.1.2. Filo Schlieric Granite

The Filo schlieric granite sample SQ17-049 was described in Section 4.1. Unlike the migmatitic country rocks, this granite has Pampean-age zircons, both in cores and rims, with only five dated rims of Famatinian age (Figure 8). The zircon grains are usually euhedral to subhedral with a 1:2 to 1:4 aspect ratio. The Pampean-age zircons either show oscillatory zoning or featureless CL texture, and their rare Famatinian-age rims are featureless or show sector zoning (Figure 5). The results show a concentration of dates between ca. 550 and 520 Ma, coinciding with Pampean-age magmatism (Rapela et al., 1998a; Schwartz et al., 2008), with outliers between 550 and 570 Ma and between 504 and 510 Ma (blue in Figure 8).

4.3.1.3. Zircon Chemistry: Th/U, Ti-In-Zircon Thermometry and Rare Earth Elements

The Pampean-age zircon analyses from the Filo schlieric granite sample SQ17-049 have Th-U ratios >0.1, whereas most of the Famatinian-age rim analyses have Th-U ratios <0.1 (Table S1), common in metamorphic

10.1029/2021TC007027

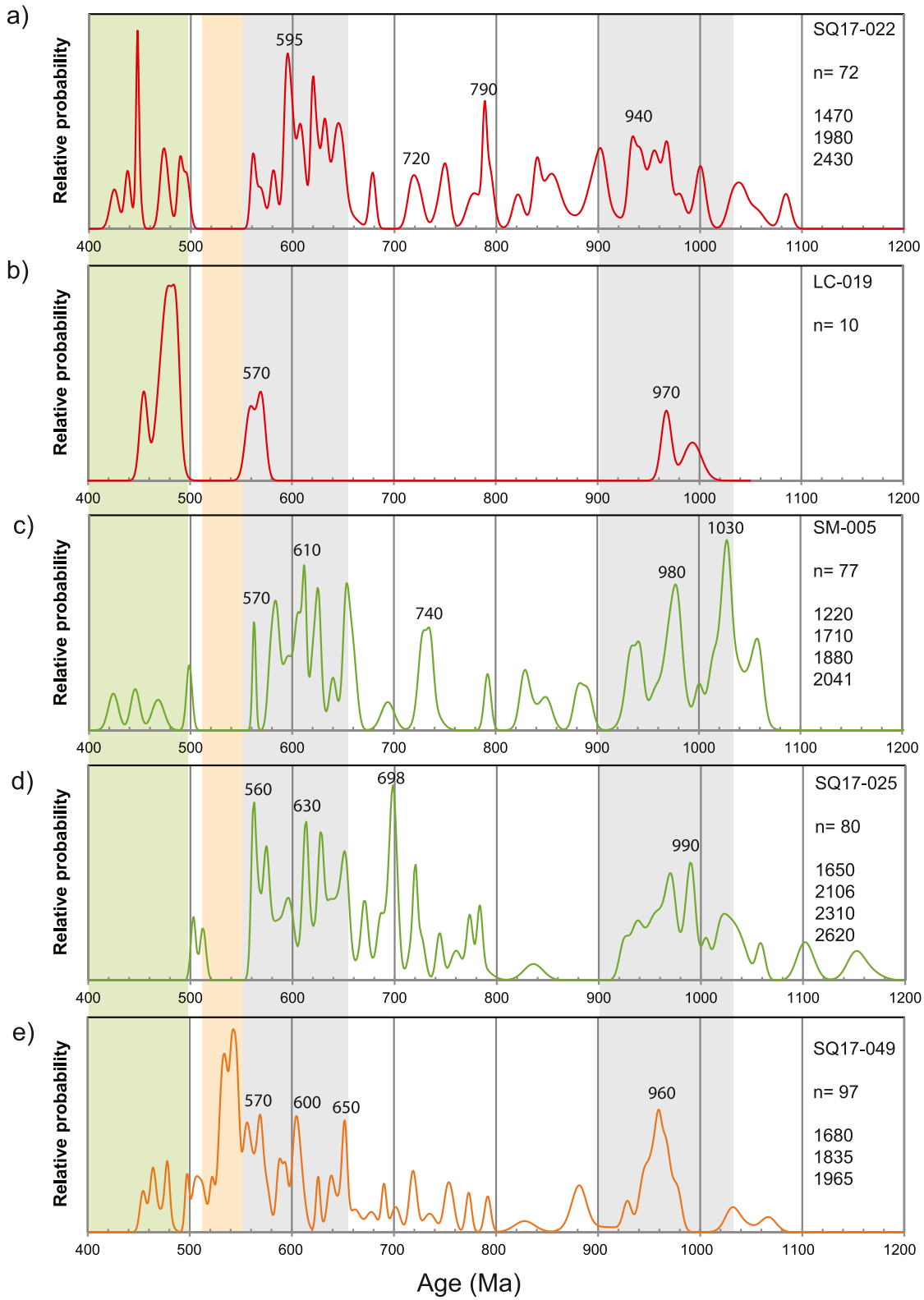

Figure 6. Probability plots of zircon dates: (a, b) for Al-rich siliciclastic rocks; (c, d) for Ca-rich siliciclastic rocks; and (e) for the Filo schlieric granite. The green vertical strip marks the duration of the Famatinian orogeny, the yellow strip the Pampean orogeny, and gray strips indicate the dominant ages of detrital zircons in the Puncoviscana sequence. The period from 515 to 500 Ma is a magmatic lull that marks the transition between the Pampean and Famatinian orogenies (Weinberg et al., 2018). The Filo schlieric granite sample SQ17-049 in (e) is the only one with Pampean zircons. Numbers on the right-hand-side of the images correspond to older age peaks not shown in the plots (in Ma). Analyses >10% discordant were not considered. Data in Table S1.

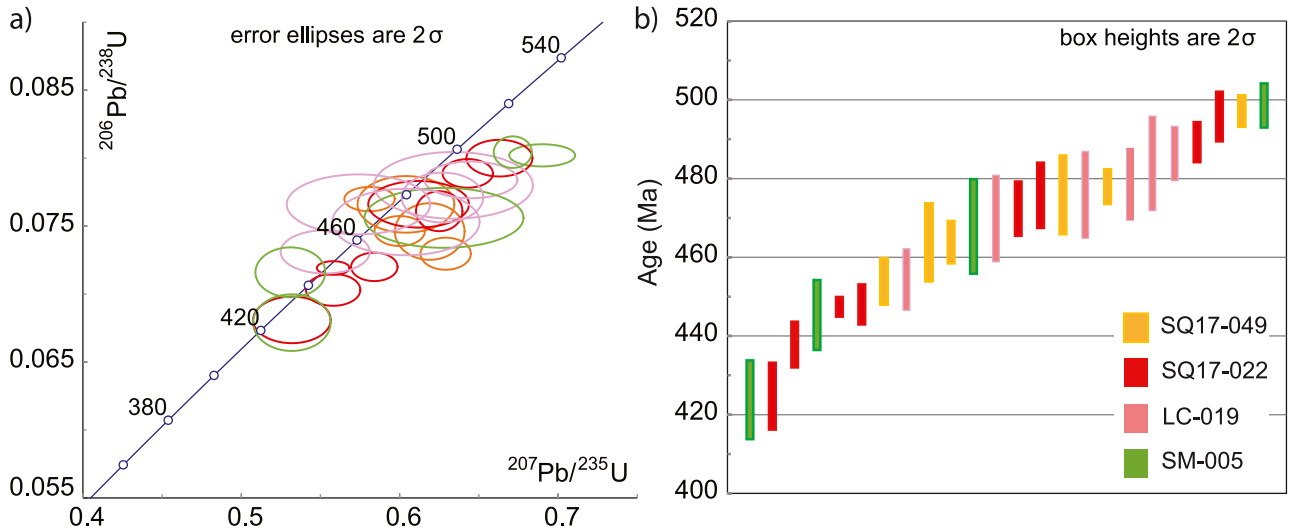

Figure 7. (a) Concordia diagram for zircon rim analyses from four samples. Some discordant grains reflect the possible effect of common-Pb. All 24 analyses are <10% discordant. (b) Spread of Famatinian $^{206}Pb/^{238}U$ dates.

zircons (Rubatto, 2002; Yakymchuk et al., 2018). These are similar to the ratios for Famatinian-age zircon analyses from migmatite samples.

Temperature estimations were obtained using Ti-in-zircon thermometry with the calibrations of Watson et al. (2006) that have an estimated uncertainty of ±10°C. This method was calibrated for rocks with rutile and $a(TiO_2) = 1$. Watson et al. (2006) argued that in the presence of other Ti-bearing mineral phases (titanite or ilmenite), titanium activity should remain high. However, Schiller and Finger (2019) concluded that for ilmenite-bearing S-type granitic magmas, a value of $a(TiO_2) = 0.5$ is more appropriate. All our samples have ilmenite and we used this lower activity to calculate the Ti-in-zircon temperatures. Table 3 lists the results. Approximately half of the analytical spots have Ti content below detection limits (not listed on the table) or large uncertainties. The few analyses obtained for the migmatites yielded Ti < 10 ppm, reflecting temperatures between 700°C and 800°C.

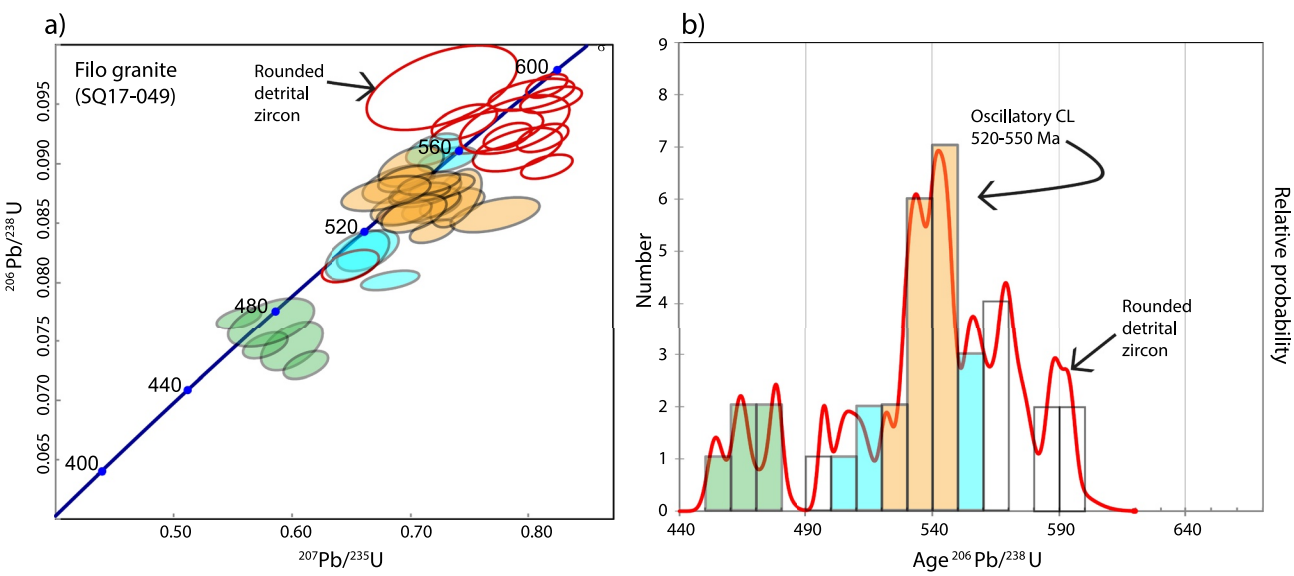

Figure 8. Zircon U-Pb dates for the Filo schlieric granite sample SQ17-049. (a) Concordia diagram, and (b) probability plot showing how the dates relate to cathodo-luminescence (CL) textures. In green Famatinian rims, in light-blue Pampean-age values derived from zircon regions with featureless CL texture, in orange Pampean-age values from zircon regions with oscillatory CL texture. Pampean and Famatinian dates that plot away from the concordia in (a) reflect common-Pb effect but all are <10% discordant. Dates older than 600 Ma are not shown.

Table 3
Ti-In-Zircon Temperature Calculated for $a(TiO_2) = 0.5$ and $a(SiO_2) = 1$ Following Schiller and Finger (2019)

Sample	Spot name	Ti (ppm)	2σ	Ti-in-zircon *T* (°C)	$^{206}Pb/^{238}U$	±
SQ17-049 Famatinian rims	49-180-2	2.6	1.6	690	454	6
	49-183-2	4.4	1.9	730	464	5
	49-222-2	6.8	3.6	780	476	10
	49-69-2	5.2	4	750	497	4
SQ17-049 Pampean cores	49-38a-1	19.9	7.2	900	510	10
	49-5-2	6.1	2.8	770	512	8
	49-35-1	4.6	2.4	740	522	5
	49-58-1	13.7	4.1	850	530	7
	49-78-1	13.9	4.3	850	535	7
	49-30-1	18.3	3.8	880	535	7
	49-40-2	19	12	890	535	5
	49-60-1	11.7	2.8	830	538	12
SQ17-022 migmatite	22-31-1	4.3	4.3	730	438	6
	22-48-22a	3	1.2	700	473	7
	22-35-2	4.4	2.5	730	489	5
SM-005 migmatite	005-11-1	8	2.7	790	499	6

Note. Also provided are the spot U-Pb dates. Note large uncertainty in Ti measurements (2σ values).

These coincide with the Famatinian rims of the Filo schlieric granite sample SQ17-049 but are markedly lower than the Pampean-age zircon spots in this same sample, which have Ti contents >10 ppm reflecting temperatures 50°C to 100°C higher.

Zircon rare earth elements (REE) was analyzed to trace contemporaneous formation or destruction of other REE-rich mineral phases such as garnet or monazite (Taylor et al., 2016, and references therein). Both the Famatinian rims of the Filo granite sample SQ17-049 and the Al-rich migmatite sample SQ17-022 have $Lu_n/Sm_n \sim 150$, with negative Eu anomaly and positive Ce anomaly and substantial dispersion of LREE values. Figure 9 compares

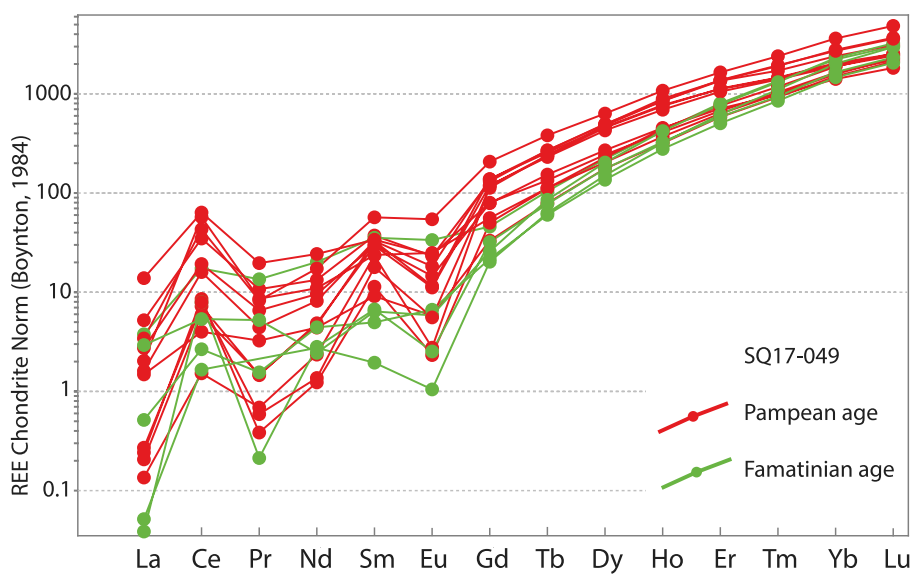

Figure 9. Chondrite normalized rare earth elements diagram for Pampean- and Famatinian-age zircon analyses from the Filo schlieric granite sample SQ17-049. Famatinian-age analyses have lower middle rare earth element values (Gd, Tb, and Dy).

the REE values of Pampean- and Famatinian-age spot analyses from sample SQ17-049. All analyses have a similarly steep REE pattern ($Lu_n/Sm_n \sim 150$). They differ in their middle rare earth element (MREE) contents where the Famatinian-age rims have lower values than Pampean ones (see Table S2).

In summary: (a) the four migmatites and the Filo schlieric granite yielded DZ cores and have maximum deposition age (MDA) of 550 Ma; three of them have thin Famatinian-age zircon rims with dates scattered between ca. 490–420 Ma, usually with Th/U < 0.1 and CL textures characteristic of metamorphic zircon; (b) the Filo schlieric granite sample SQ17-049 has Pampean-age zircons, absent in all four migmatite samples, with oscillatory CL texture and Th/U > 0.1, typical of igneous zircon; (c) Ti-in-zircon temperatures calculated from Pampean-age areas in zircons are 50°C–100°C higher than the Famatinian-age rims that range between 700°C and 800°C. The latter coincide with Zr-in-titanite temperatures determined for the same rocks (Farias et al., 2020).

4.3.2. Monazite

A total of four samples were selected for monazite dating. Samples SQ17-049 and SQ17-022 were dated by means of LASS-ICP-MS and samples SM-003 and LC-019 by LA-ICP-MS (results are in Table S3). Except for SM-003, they all had their zircon dates described in the previous section. Monazite grains were hand-picked and separated based on color, shape, and size. Most are light amber in color, roughly rounded and 100–150 μm in diameter. The BSE images show no internal zonation, however most grains where more than one spot was analyzed yielded variable U-Pb dates.

Dates were calculated and plotted using the package IsoplotR 4.2 (Vermeesch, 2018) in R 4.0.3 (R Core, 2020) running in RStudio 1.4.1717. Sixty-three monazite grains were dated for leucosome sample SQ17-022, with a total of 63 analyses. Thirty-eight out of the total are 100% concordant, and the remaining are less than 5% discordant (Figure 10a). The dates range between 444 and 465 Ma. All analyses yield a mean age of 456 ± 1 Ma, [MSWD] = 0.8 and a probability of fit [p] = 0.8.

Eighty-six monazite grains were dated for the Filo schlieric granite sample SQ17-049, and a total of 89 spots analyzed (Figure 10b). All analyses are <5% discordant and yield a spread of dates between 447 and 467 Ma with a mean age of 458 ± 1 Ma, [MSWD] = 0.8 and [p] = 0.9. Twelve monazite grains with a total of 20 spots were analyzed for sample LC-019. The analyses are all <3% discordant (Figure 10c). The dates range between 442 and 492 Ma. The weighted average is not meaningful due to the large spread and [MSWD] = 8.3 and [p] = 0.0. Twenty-nine monazite grains from sample SM-003 were analyzed with a total of 45 spots (Figure 10d). The dates range between 417 and 471 Ma, with a mean of 454 ± 1 Ma, [MSWD] = 7 and [p] = 0.0. These include three young data points. When these are removed the data defines a mean of 456 ± 1 Ma with [MSWD] = 3.7 and [p] = 0.0.

The Filo schlieric granite SQ17-049 and the leucosome SQ17-022 have the narrowest distribution, with dates varying between 445 and 465 Ma and coincident means at 457 ± 1 Ma. Metatexite sample SM-003 also has a well-defined date concentration at this time (456 ± 1), accompanied by dates younger than 440 Ma. The metatexite sample LC-019 does not define a clear mean age possibly as a result of few analyses. The monazite date distribution mostly overlaps with those of their Famatinian zircon counterparts, but they are older than sample SQ-181a in Finch et al. (2017), which defines a broad peak between 440 and 410 Ma. This younger date overlaps only with a small number of analyses from sample SM-003.

4.3.3. Titanite: Zr-In-Titanite Thermometry and REE Evolution

LASS-ICP-MS U-Pb dates for 454 spots in titanites from seven different Ca-rich siliciclastic rocks of the Agua del Sapo complex have been published in Farias et al. (2020). They yielded a range of dates between 500 and 380 Ma, extending the range obtained for monazite (Figure 10) to both older and younger values. Two populations were defined by titanites defining three different types of date distribution: three samples yielded a unimodal distribution between 500 and 440 Ma, centered around 460 Ma, whereas two samples yielded a broad peak of younger dates between 440 and 380 Ma with a trail of spots older than 440 Ma. The two remaining samples covered the entire range from 500 to 380 Ma.

Farias et al. (2020) reported also on Zr-in-titanite thermometry (Hayden et al., 2008) from these samples assuming constant P at 5.5 kbar. Results demonstrate that the Agua del Sapo complex remained above 700°C for 120 Myr, defining a curve with temperatures gently increasing from 700°C toward a maximum of 750°C at around 460 Ma followed by a slow cooling starting at ~440 Ma reaching 700°C at 380 Ma (with uncertainty of 25°C for indi-

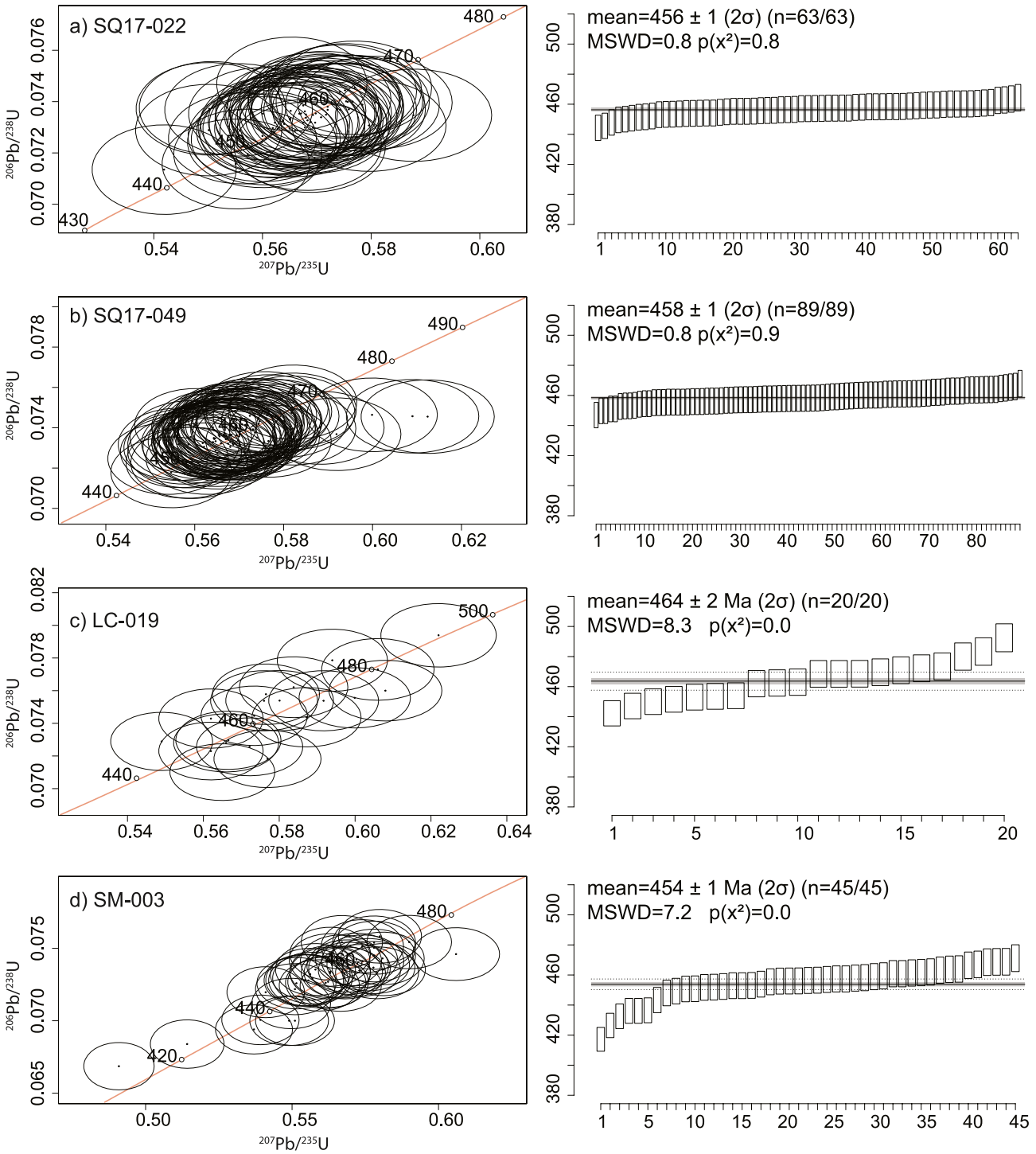

Figure 10. Concordia diagram (left) and weighted average diagram (right) for monazite U-Pb results for samples: (a) SQ17-022; (b) SQ17-049; (c) LC-019; and (d) SM-003. All error ellipses and bars are 2% of the central date (Table S3).

vidual measurements). The results are in line with the Ti-in-zircon temperatures mentioned above, and contrast with those of an Opx-bearing migmatite from the Tolombon complex that yielded Zr-in-titanite temperatures of 800°C–850°C (Figure 11a) that confirm the peak temperatures estimated by Büttner et al. (2005). Pressure could have varied over this prolonged period and could affect the calculated temperatures. Here, we explore the REE pattern of these same titanites (data in Table S4).

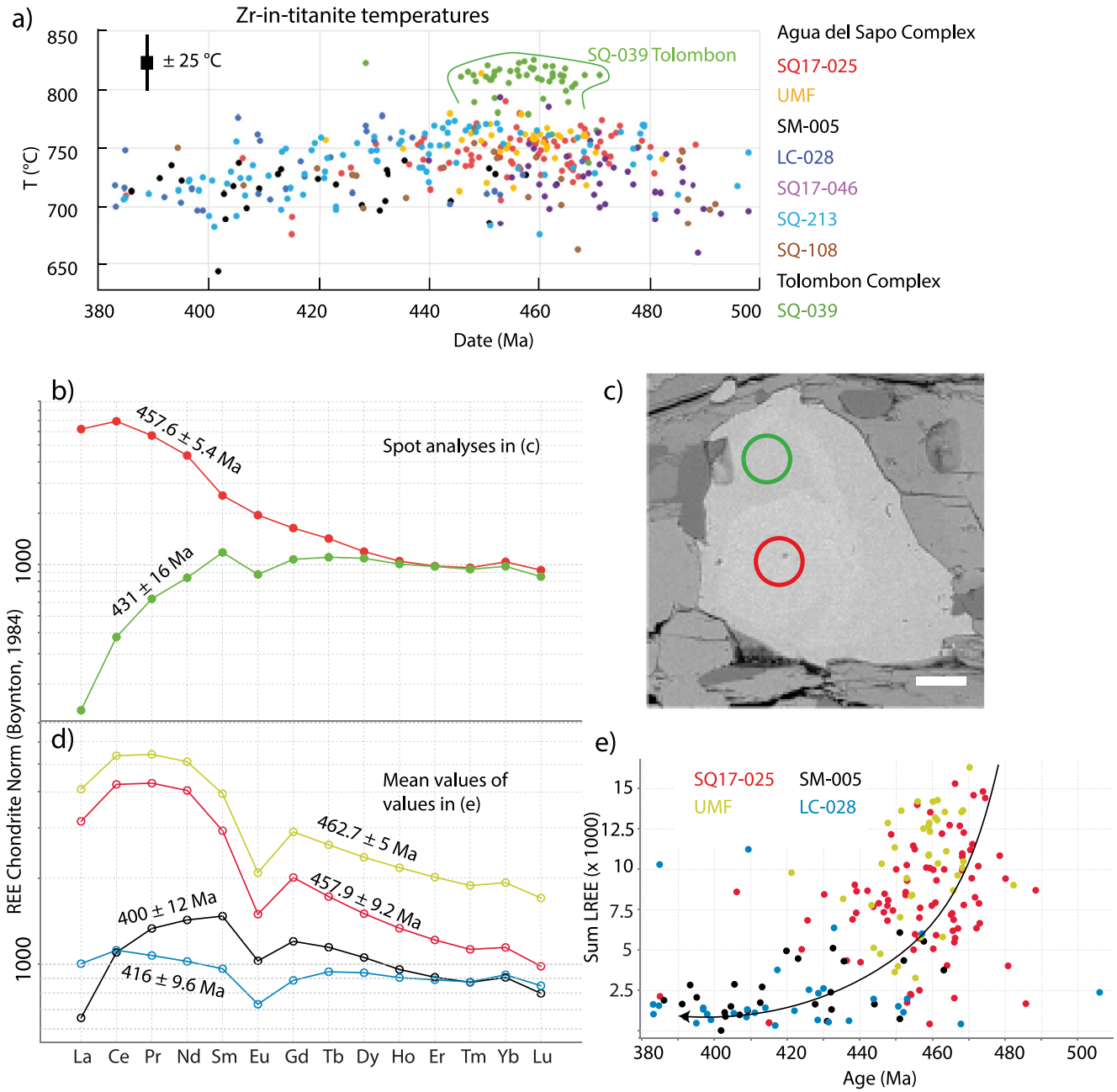

Figure 11. (a) Zr-in-titanite thermometry (modified from Farias et al., 2020). Note the higher temperatures for the Opx-bearing migmatite from the Tolombon complex sample SQ-039. (b) Rare earth elements (REE) chondrite normalized diagram for two spots in zoned titanite grain in (c) from sample SQ-213. (c) Bright zone in the core is older and have higher light rare earth element (LREE) (in red) compared to the younger dark zone (in green). Scale bar in backscattered electrons image is 25 μm. (d) Comparison between REE contents for different mean ages. Samples younger than 440 Ma have lower REE, specially LREE. (e) Sum of LREE content in titanite as a function of spot U-Pb date defining a positive trend.

Titanite grains commonly have bright BSE cores and darker rims. The brighter cores are older, and have higher total REE, in particular LREE, and higher $(La/Lu)_N$ than the dark rim zones (Figures 11b and 11c). The same pattern was found for entire sample averages: samples with older mean ages have higher REE contents (Figure 11d). Figure 11e shows a systematic increase in the LREE content of titanite as the date increases, defining a positive trend.

We used polynomial fits for the REE curves and defined the λ shape coefficients of O'Neill (2016) to compare the curves for each analysis as a function of time. We used λ_1, the coefficient that describes the slope of the REE

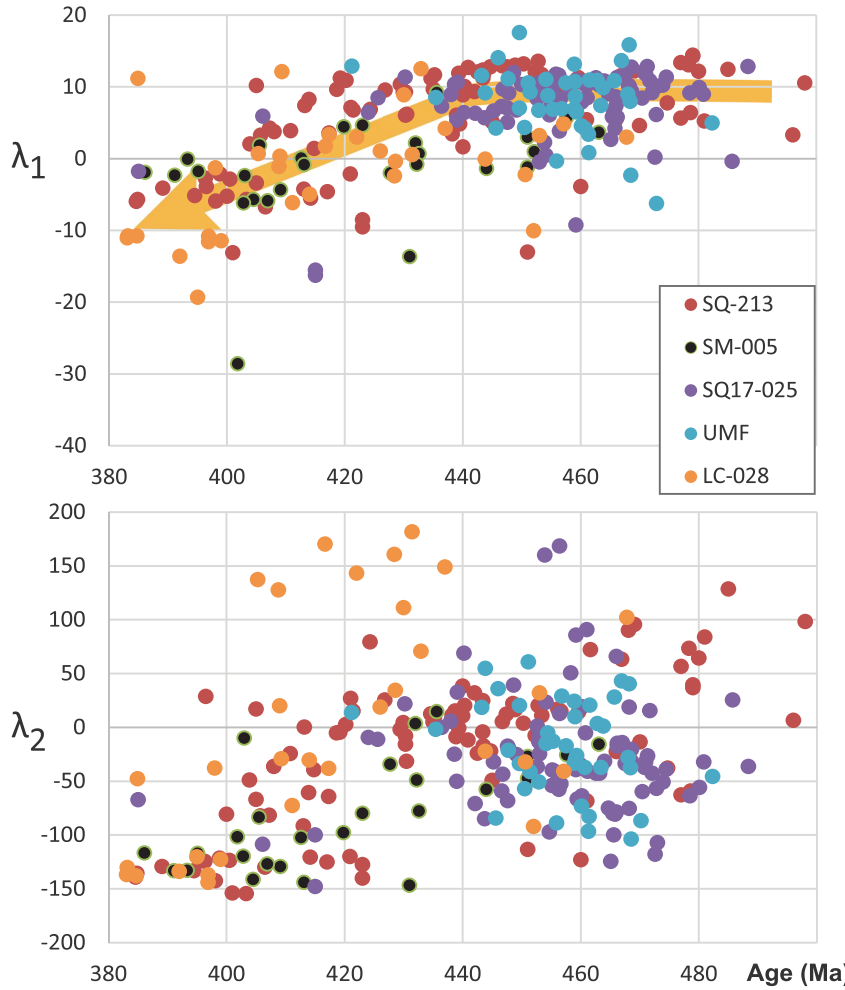

Figure 12. λ_1 and λ_2 versus spot U-Pb dates for titanite. λ_1 shows relatively constant values of 0–10 between 480 and 440 Ma followed by a decrease reaching negative values by 410 Ma. Note that some samples cover the entire range of dates (e.g., SQ-213 in red-brown), whereas others cover only part of the range (e.g., UMF covers the older half; and SM-005 covers the younger half). λ_2 is more scattered but indicates that the rare earth elements curves become more concave downwards (∩) with time, indicated by negative λ_2 values. This change reflects the decrease in light rare earth element values with time.

pattern (LREE-enriched curves have a positive λ_1), and λ_2, that describes the quadratic curvature where a positive value describes a concave-upwards curve, and a negative value describes a concave-downwards curve. For our samples, both λ_1 and λ_2 change as a function of time. Figure 12 shows a relatively constant λ_1 from 480 to 440 Ma at which point it starts falling, reaching negative values at ~410 Ma. This is accompanied by a less well-defined increase in the concavity of the curve recorded by decreasing negative values of λ_2.

5. Discussion

5.1. Maximum Depositional Age of the Sedimentary Sequence

The youngest detrital zircons in the meta-turbidite migmatites of the Agua del Sapo complex are dated at 550 Ma, defining the maximum depositional age (MDA; Figure 6) (Gehrels, 2014). This contrasts with their counterparts in the hanging wall Tolombon complex, which contains Pampean-age detrital zircons and an MDA of ~520–510 Ma (Finch et al., 2021). The DZ dates match those of the Puncoviscana sequence having two important age groups: the late Mesoproterozoic-early Neoproterozoic (1,200–900 Ma) and the Neoproterozoic-Early Cambrian (670–545 Ma) (Miller et al., 2011), as well as minor Paleo- to Mesoproterozoic peaks (Adams et al., 2011; Escayola et al., 2011; Hauser et al., 2011; Miller et al., 2011; Schwartz & Gromet, 2004). Some authors extended the Puncoviscana sequence to include rocks with zircons as young as 520 Ma sourced from the

Pampean arc, such as the Tolombon complex (Adams et al., 2011; Hauser et al., 2011; Rapela et al., 2016; Sims et al., 1998). The absence of Pampean-age zircons in the Agua del Sapo complex samples (Figure 6) suggests either that the parental sediments of the migmatites were deposited before the onset of the Pampean magmatic arc, or that they were absent from the sediment catchment area.

5.2. Origin of the Filo Schlieric Granites: Pampean-Age Intrusions

Sample SQ17-049 of the Filo granite is the only one with Pampean-age zircons. We consider two possible explanations: (a) that this is the crystallization age of the granite, and that the younger zircon rims and monazite dates represent Famatinian high-grade metamorphism; or (b) that the Pampean dates are inherited from the magma source and the Famatinian rims record granite crystallization. Alternative (a) is favored because: the host migmatites surrounding the Filo granite, the most likely potential source, lack Pampean-age zircon or monazite; and the Pampean-age zircons have igneous morphology (euhedral and with 1:2 to 1:4 aspect ratios), oscillatory zoning, and Th/U typically >0.1 (Figure 5) (Hoskin & Schaltegger, 2003; Rubatto, 2002; Taylor et al., 2016). This contrasts with the Famatinian zircon rims that have metamorphic features such as ill-defined zonation and Th/U < 0.1 (Hoskin & Black, 2000; Hoskin & Schaltegger, 2003; Taylor et al., 2016).

The absence of Pampean-age zircon in the turbidites of the Agua del Sapo complex implies that Pampean metamorphism was not sufficiently hot to trigger significant melting and growth of zircons. This is the case more broadly for the Sierra de Quilmes where the record of Pampean high-grade metamorphism is missing (Büttner et al., 2005; Lucassen et al., 2000, 2011). We conclude that the Filo schlieric granite is a 550–520 Ma Pampean intrusion (Figure 8) intruded into Puncoviscana low-grade meta-sedimentary rocks. These rocks were subsequently heated during the Famatinian orogeny when anatexis led to growth of the metamorphic zircon rims in the Filo granite.

Interestingly, this granite is located in the Pampean fore-arc, ∼100 km west of the magmatic arc, and this is in line with the Pampean-age granites (550–525 Ma; ID-TIMS and LA-ICP-MS dates) found even further west of the Pampean arc in the Sierra de Fiambalá (Grissom et al., 1998; Larrovere et al., 2021; Safipour et al., 2015). In this area too, Pampean peraluminous granites (Larrovere et al., 2021) intruded greenschist-amphibolite facies rocks that were later overprinted by Famatinian-age migmatization (Grissom et al., 1998). These findings add weight to the hypothesis of Schwartz et al. (2008), that the subduction of a mid-ocean ridge was responsible for heating (Lucassen et al., 2011) and peraluminous magmatism in the fore-arc (discussed in Weinberg et al., 2018).

5.3. Famatinian Metamorphism

5.3.1. Pressure-Temperature Constraints

Our thermodynamic modeling (Figure 4), indicates that the peak mineral assemblage of the Al-rich siliciclastic migmatites in the core of the Agua del Sapo complex equilibrated between 740°C and 710°C. These temperatures are supported by both Ti-in-zircon and Zr-in-titanite thermometry, which yield temperatures between 700°C and 800°C. The decrease in temperatures from ∼750°C to ∼700°C from 440 to 380 Ma indicated by Zr-in-titanite (Figure 11)(Farias et al., 2020) defines a period of slow cooling at a rate of ∼1°C/Ma, and suggests sustained heating of the crust way beyond the accepted end of the Famatinian orogeny between 460 and 440 Ma. Slow cooling at high temperatures might have erased growth zoning of garnets in the migmatites (Caddick et al., 2010), their existence (see Section 4.2) potentially contradicts our findings and needs further investigation.

Overthrusting of the Tolombon complex (Finch et al., 2015) could have contributed to the long duration of high-temperature conditions in the footwall Agua del Sapo complex. The sustained temperatures at or above 700°C in the footwall enabled zircon rim growth, and titanite and monazite to respond to the evolving metamorphism, deformation and fluid flow conditions.

In order to better understand the titanite record, we have first checked if there was an obvious difference between samples yielding different date ranges. We found that all samples have the same mineral paragenesis, similar bulk geochemistry, and microstructures indicative of shearing. For example, migmatite sample SM-005 has dates typically <440 Ma, whereas sample SQ17-025 from a similar rock type has dates typically >440 Ma (Figure 12). This same sample has similar dates to that of the unmelted mylonite sample UMF, indicating that dates are independent of the metamorphic facies or the presence of melt. Like for monazite, the cause of titanite growth

after 440 Ma in some samples but not others, remains inconclusive but likely reflects local differences in fluid availability and deformation.

The possibility of Pb and Zr diffusion in titanites from de Agua del Sapo complex affecting the dates and thermometry has been discussed in Farias et al. (2020). They found that there is no systematic variation of U-Pb dates with either grain size or position of the analytical spot within the grain, and that even titanite grains as small as 50 μm preserve the entire 120 Myr range of dates. They concluded that because of the high closure temperature of titanite and because it is reactive during metamorphism (Scott & St-Onge, 1995), the date range and Zr-content are likely controlled by the growth of new titanite, rather than by diffusion in older grains (Frost et al., 2001). They concluded further that the younger titanite group (440–380 Ma) recorded protracted growth as a result of fluid flow, deformation, and/or metamorphic reactions (Lucassen & Becchio, 2003; Schwartz et al., 2016; Stearns et al., 2015) during the gentle cooling, marking the early stage of retrogression.

Could this protracted date distribution be a result of titanite recrystallization due to deformation? Gordon et al. (2021), investigating titanite recrystallized into aggregates by deformation, showed how U-Pb dates were reset while Zr and REE were not, leading to a decoupling between dates and the trace elements. If this was the case for the Agua del Sapo, recrystallization would have extended the titanite dates without changing Zr contents implying that Zr-based thermometry would reflect the temperatures before decoupling (see also Kavanagh-Lepage et al., 2023; Moser et al., 2022). However, for the Agua del Sapo rocks, the preserved titanite zonation and common euhedral grains (e.g., Figure 3d), the simultaneous decrease in Zr and REE contents with U-Pb dates associated with cores and rims (Figure 11) all combined, indicate that titanite deformation was negligible and unlikely to have caused U-Pb resetting and decoupling from Zr.

Figure 11 shows how the REE contents of titanite started decreasing when the temperature recorded by Zr started to drop. Angiboust and Harlov (2017) found by means of experiments, that Ca-rich rocks (~3 wt.% CaO) at pressures <7 kbar form titanite rimming ilmenite, and REE-rich epidote rimming allanite cores. Both textures are common in our Ca-rich samples (Figure 3) (CaO >2 wt.%, whole-rock chemistry is given in Table S5). Those authors found that the REE released during prograde dissolution of allanite are partially incorporated by newly formed titanite. Papapavlou et al. (2017) suggested that the low LREE content in titanite could be a result of contemporaneous growth of allanite, which has larger equilibrium partition coefficients than titanite (Garber et al., 2017; Regis et al., 2012), sequestering LREE. Based on these findings, we suggest that the titanites of the Agua del Sapo complex date the gentle cooling where retrogression led to the increase in allanite and epidote modal content taking in LREE (Figure 13).

5.3.2. Famatinian Zircon and Monazite U-Pb Dates

Unlike zircons from the Tolombon complex where entire grains yield Famatinian dates, zircons from the Agua del Sapo complex only have a few Famatinian rims wide enough for the analytical spot (24 out of 278 analyses; Figure 7). This difference is likely a result of the higher temperatures of >800°C in the Tolombon (Farias et al., 2020; Finch et al., 2017), compared to the 700°C–750°C for the Agua del Sapo complex (Figures 4, 11, and 13, and Farias et al., 2020). The higher temperatures in the Tolombon complex were accompanied by larger melt volumes and greater zircon rim volumes (Mintrone et al., 2020).

Despite this limited data set, zircon shows concordant dates between ca. 500 and 420 Ma (Figure 7). This range matches that found for monazite while titanite dates continues to 380 Ma. A wide spread of zircon dates was also found for three samples of migmatites and a granite from the Tolombon complex above the thrust that separates it from the Agua del Sapo complex (Finch et al., 2021). We would expect the hanging wall to cool before the footwall and yet one hanging wall sample records dates down to 420 Ma and the other three reach 400 Ma. The long duration of zircon growth in both the hanging and footwall complexes supports our inference of a prolonged period of high-grade metamorphism and reinforces our interpretation of the titanite results.

Could the spread of zircon dates result from Pb-loss? The closure temperature, T_c, for diffusion of Pb in zircon is typically in excess of 900°C for a typical 100-μm-long zircon grain and a cooling rate of 10°C/Ma (Cherniak & Watson, 2001; Lee et al., 1997). Zircons that remain above 600°C–650°C will be continuously annealed and lattice damage will not accumulate (Cherniak, 2010; Cherniak & Watson, 2001; Mezger & Krogstad, 1997), hence preventing Pb-loss. Based on the mineral paragenesis and thermodynamic modeling (Section 3.4), the Agua del Sapo complex is interpreted to have reached temperatures above 700°C, and Zr-in-titanite thermometry

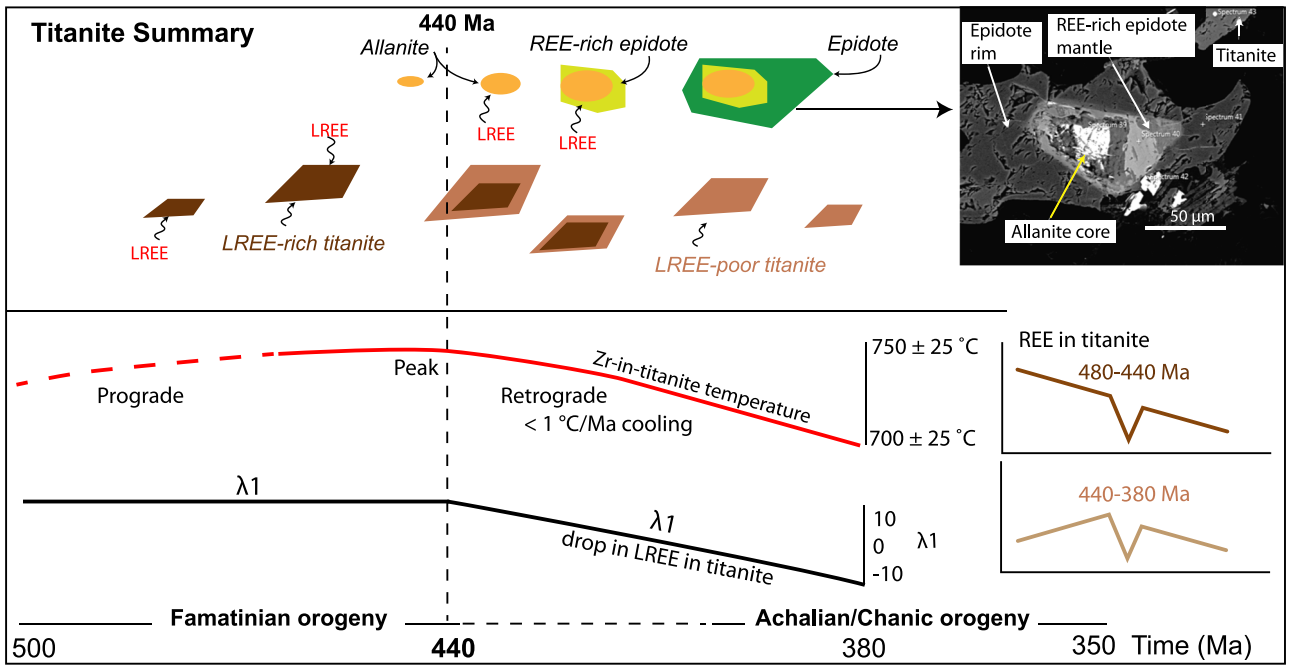

Figure 13. 120 Myr evolution inferred from titanite dates and rare earth elements (REE) composition. During peak metamorphic conditions before 440 Ma, titanite takes in available light rare earth element (LREE) (dark brown lozenges). After 440 Ma, as temperature slowly decreases below 750°C, allanite-epidote are stabilized and become the preferred sink for LREE. New titanite becomes depleted in LREE (light brown lozenges) recorded by a decrease in REE $\lambda 1$ values (black line) that go from positive to negative (from Figure 12). The allanite cores mantled by REE-rich epidote rimmed by epidote (SEM image in the top right-hand side of figure), indicate the progressive depletion of available LREE during retrogression.

suggests that these rocks may have remained at such temperatures from ca. 500 to 380 Ma (Figure 11), with no evidence for metamictization and Pb-loss during this period. However, after 380 Ma, zircons resided at lower temperatures and accumulated damage accounting for possible late Pb-loss. Despite this possibility, we interpret the Famatinian zircon dates in Figure 7 as reflecting rim growth during prolonged metamorphism (see also Wolfram et al., 2019).

Monazite from the same samples yielded Famatinian ages in cores and rims and three samples define a peak centered at 457 Ma and the fourth (LC-019), with only 20 analyses, does not define a peak (Figure 10c). One of the samples defining a 457 Ma peak, sample LC-003, has a trail of younger dates that overlap with those from sample SQ-181a from Finch et al. (2017) ranging between 440 and 410 Ma. Differences in the range of dates between the samples could be a combined result of differences in rock chemistry (e.g., P + REE contents) modulated by variations in metamorphic conditions. However, the results do not seem overly sensitive to either. For example, the two samples with dates <440 Ma are from Al-rich rocks with different metamorphic facies: the unmelted amphibolite facies sample SQ-181a, and the migmatite sample LC-003, while the samples with well-defined date concentrations at ca. 457 Ma are from Ca-rich protoliths (samples SQ17-049 and SQ17-022) and from Al-rich ones (sample SM-003). Gardés et al. (2007) confirmed that Pb diffusion is too slow at typical metamorphic temperatures to alter U-Th-Pb dates in monazite. Prolonged periods at temperatures above 900°C are necessary for diffusion rates to alter trace element composition (Cherniak & Pyle, 2008; Cherniak et al., 2004). However, coupled dissolution-precipitation mechanisms can give rise to new monazite with perturbed dates due to incomplete radiogenic Pb dissolution (Catlos et al., 2010; Harlov & Hetherington, 2010; Hetherington et al., 2010; Seydoux-Guillaume et al., 2003, 2019; Teufel & Heinrich, 1997; Williams et al., 2011). This process was used to explain the 50 Myr spread of monazite dates in the Tolombon complex found in both rim and cores of individual grains (Weinberg et al., 2020). The same is used here to interpret the spread of dates found for sample SM-003 and to argue that the spread toward 410 Ma records a protracted tectonothermal event.

While the range of monazite dates matches those in the Tolombon complex (Finch et al., 2017; Weinberg et al., 2020), they yield well-defined central ages at ~457 Ma, absent for Tolombon samples. This age does not match the broad peak between 440 and 410 Ma of sample SQ-181a from Finch et al. (2017). The results for this

sample, together with the few analyses younger than 440 Ma from sample SM-003 (Figure 10d), support the titanite record of continued high-temperature and deformation beyond 440 Ma.

These results for monazite raise questions about why the record of dates <440 Ma is so patchy. In addition to temperature, the rock fabric, interstitial fluid flow and shearing can impact on growth or coupled dissolution-precipitation of reactive accessory phases (Mahan et al., 2006; Rolland et al., 2003; Wawrzenitz et al., 2015; Williams et al., 2007). Kelsey et al. (2008) and Yakymchuk and Brown (2014) modeled pelitic metasedimentary rocks similar to ours and found that temperature and LREE content of the rock are the critical factors controlling the formation or dissolution of monazite during metamorphism. Kelsey et al. (2008) defined "effective LREE content" as the fraction of the bulk LREE content of the rock that interacts with monazite. Effective LREE content is controlled mainly by the breakdown of LREE-bearing minerals (e.g., allanite-epidote, titanite). The bulk LREE contents of three of our four monazite whole-rock samples are similar: metatexite SM-003, leucosome SQ17-022 and Filo granite SQ17-049 have 195, 163, and 177 ppm LREE, respectively (Table S5). If we assume that they all reached similar peak temperatures, we should expect similar monazite date distribution. However, the weakly deformed and coarse-grained granite (SQ17-049) and leucosome (SQ17-022) samples have a much narrower date range than the metatexite SM-003 (Figure 10). This could reflect differences in the "effective LREE" contents of the rocks.

In summary, while zircon responded to Famatinian-age anatexis with the growth of narrow rims, ranging from 500 to 420 Ma, on detrital cores, monazite was either completely reset or grew entirely during the Famatinian event, lacking inherited ages. Three samples define a peak at ~457 Ma. This peak of monazite growth is unlikely to reflect a pronounced thermal peak and instead records the time when ideal conditions for monazite growth were reached reflecting ideal temperature, fluids and deformation conditions. The one sample with younger monazite dates (SM-003) suggests that at least some monazite grains may have experienced coupled dissolution-precipitation (Foster et al., 2002; Seydoux-Guillaume et al., 2003; Weinberg et al., 2020). In contrast to monazite and zircon, titanite continued to grow in some samples to 380 Ma during cooling from ~750°C to ~700°C.

5.4. Famatinian Retro-Arc: Blurring the Boundary to the Achalian/Chanic Orogen

While there is robust evidence for magmatism and anatexis in the retro-arc of the Famatinian orogen between ca. 505 and 440 Ma (e.g., Table 1 in Bahlburg & Berndt, 2016; Wolfram et al., 2019), evidence for high temperature after 440 Ma is less well-defined. In the southern Puna, Lucassen et al. (2011) reported high-temperatures (600°C–750°C) at ~ 5–7 kb from 470 to 420 Ma. In the southern Sierras Pampeanas, near the contact between the MARA terrane and the Famatinian arc, Mulcahy et al. (2014) found that suprasolidus temperatures were sustained for ca. 30 Myr after peak metamorphism at ca. 460 Ma, followed by near-isobaric cooling from ~850°C at ca. 465 Ma, to ~650°C at ca. 407 Ma (~4°C/Ma), similar to the cooling rate estimates of Gallien et al. (2010) and Cristofolini et al. (2014). In the MARA terrane of the WSP, metamorphism and deformation in the Sierras de Ramadita and Maz record a Silurian event between 450 and 410 Ma (Lucassen & Becchio, 2003; Martin et al., 2019; Tholt et al., 2021). This event has been referred to as the Rinconada tectonic phase of the Famatinian orogeny (Casquet, Ramacciotti, et al., 2021; Verdecchia et al., 2022). Our results support these recent findings and extend this event into the ESP, the retro-arc of the Famatinian orogeny.

There remains the question of the heat source for this sustained heating. The discussion in Wolfram et al. (2019) is pertinent here. They argued that because the high temperatures remained virtually unchanged as deformation changed from the early extensional to the shortening phase of the Famatinian orogeny, heating most likely reflected forced convection of the asthenospheric mantle wedge in response to subduction, directing heat toward the back-arc (Curie & Hyndman, 2006). They also argued that basaltic underplating of the crust was required to maintain the long-lived high-T/low-P metamorphism.

6. Summary and Conclusions

Integration of U-Pb dates and composition from zircon and monazite with those of titanite reveals a number of features of the evolution of the Agua del Sapo complex. Detrital zircon of the migmatitic sequence indicates that they derive from the turbidites of the Puncoviscana sequence lacking Pampean-age DZ (550–520 Ma). This contrasts with the migmatitic turbidites of the hanging wall Tolombon complex, which have these zircons and

therefore may have been deposited contemporaneously with the Pampean magmatic arc activity. The lack of Pampean-age zircon or monazite suggests that the Agua del Sapo metaturbidites remained at subsolidus conditions during the Pampean orogeny while it was intruded by the Pampean-age Filo schlieric granites. Magmatism in what would have been the fore-arc to the west of the main Pampean arc, is in line with the findings of Larrovere et al. (2021) and suggests subduction of a mid-ocean ridge during the Pampean orogeny (Schwartz et al., 2008).

The onset of the Famatinian orogenic cycle is marked by HT-LP metamorphism recorded by zircon, monazite and titanite dates. While most of the data record the expected 500–440 Ma range for the Famatinian orogen, some zircon rims and monazite grains yield younger dates and titanite dates continues to 380 Ma, extending the Famatinian metamorphism into the Achalian/Chanic orogeny. The combined use of metamorphic modeling, Ti-in-zircon and Zr-in-titanite geothermometers constrained the thermal evolution of this long-lived metamorphism where temperatures reached maximum values of ∼750°C at ca. 460 to 440 Ma and then slowly decreased by ∼ 1°C/Ma reaching ∼700°C at 380 Ma.

During this prolonged metamorphic event, the geochronometers reacted in different ways to the evolving thermal, deformational and fluid regimes. Zircon gained only relatively rare and thin metamorphic rims, in contrast with the zircons from the Tolombon complex that record at least 50°C hotter metamorphism and where newly-formed Famatinian zircon grains are common. We ascribe this difference to the lower temperatures in the Agua del Sapo complex, leading to lower melt fractions, less dissolution of DZ grains and hence narrow newly grown rims.

Monazite in the Tolombon complex, in the hanging wall of the thrust, underwent coupled dissolution-precipitation that perturbed its date record and the coupling between individual dates and internal grain zonation (Weinberg et al., 2020). In the Agua del Sapo complex in the footwall, three samples of unzoned monazite define a narrow peak at ∼457 Ma, with only one of them extending to dates younger than 440 Ma, overlapping with those in Finch et al. (2017). This suggests that the U-Pb systematics in monazite may have been better preserved at the lower temperatures of the footwall than the hanging wall. Nevertheless, the results indicate that in some samples monazite remained open to 410 Ma, possibly reflecting active coupled dissolution-precipitation.

Of the three accessories, titanite provides the most complete record with dates ranging from 500 to 380 Ma. The changes in REE contents and Zr-in-titanite thermometry are interpreted together as recording both the prograde and the slow-cooling retrograde sections of the thermal history of the Agua del Sapo complex. At the point when Zr-in-titanite thermometry indicates that temperatures started to decrease, the REE contents, specially LREE, also started to decrease. A possible explanation is that cooling led to increased modal contents of Aln + Ep, taking the REE and leaving titanites impoverished. The 120 Ma-long growth record of titanite suggests that it remained reactive to changes in its surroundings long after the closure of zircon and monazite. The sustained high-temperatures through to 380 Ma indicates that the Rinconada tectonic phase described in the WSP (e.g., Casquet, Ramacciotti, et al., 2021), extends to the ESP, and blurs the gap between the Famatinian and the Achalian/Chanic orogen (Ramos et al., 1986; Rapela et al., 1998a; Sims et al., 1998).

Conflict of Interest

The authors declare no conflicts of interest relevant to this study.

Data Availability Statement

The data obtained for this paper can be found in the Supporting Information and available via DOI (https://doi.org/10.4121/15153594).

Acknowledgments

We thank Tato Becchio and Nestor Suzaño for discussions and a great time in the field. We thank Massimo Raveggi and Vitor Barrote for technical support. We would also like to thank the very careful and helpful reviews by Kathryn Cutts, Oscar Laurent, Friedrich Lucassen and an anonymous reviewer, and the handling of associate editor Djordje Grujic. A. Sola thanks the Agencia Nacional de Promoción Científica y Tecnológica for the Grant PICT-2018-02889 (FONCyT). This research was supported by the Australian Research Council Grant DP110102543 to R.F.W. Open access publishing facilitated by Monash University, as part of the Wiley - Monash University agreement via the Council of Australian University Librarians.

References

Aceñolaza, F. G., Miller, H., & Toselli, A. J. (2002). Proterozoic–early Paleozoic evolution in western South America—A discussion. *Tectonophysics*, *354*(1–2), 121–137. https://doi.org/10.1016/s0040-1951(02)00295-0

Adams, C. J., Miller, H., Aceñolaza, F. G., Toselli, A. J., & Griffin, W. L. (2011). The Pacific Gondwana margin in the late Neoproterozoic–early Paleozoic: Detrital zircon U–Pb ages from metasediments in northwest Argentina reveal their maximum age, provenance and tectonic setting. *Gondwana Research*, *19*(1), 71–83. https://doi.org/10.1016/j.gr.2010.05.002

Aleinikoff, J. N., Schenck, W. S., Plank, M. O., Srogi, L. A., Fanning, C. M., Kamo, S. L., & Bosbyshell, H. (2006). Deciphering igneous and metamorphic events in high-grade rocks of the Wilmington complex, Delaware: Morphology, cathodoluminescence and backscattered electron

zoning, and SHRIMP U-Pb geochronology of zircon and monazite. *Bulletin of the Geological Society of America*, *118*(1–2), 39–64. https://doi.org/10.1130/b25659.1

Angiboust, S., & Harlov, D. (2017). Ilmenite breakdown and rutile-titanite stability in metagranitoids: Natural observations and experimental results. *American Mineralogist*, *102*(8), 1696–1708. https://doi.org/10.2138/am-2017-6064

Astini, R. A. (1998). *Stratigraphical evidence supporting the rifting, drifting and collision of the Laurentian Precordillera terrane of western Argentina* (Vol. 142, pp. 11–33). Geological Society, London, Special Publications.

Astini, R. A., Benedetto, J. L., & Vaccari, N. E. (1995). The early Paleozoic evolution of the Argentine Precordillera as a Laurentian rifted, drifted, and collided terrane: A geodynamic model. *Bulletin of the Geological Society of America*, *107*(3), 253–273. https://doi.org/10.1130/0016-7606(1995)107<0253:tepeot>2.3.co;2

Astini, R. A., & Dávila, F. M. (2004). Ordovician back arc foreland and Ocloyic thrust belt development on the western Gondwana margin as a response to Precordillera terrane accretion. *Tectonics*, *23*(4), 4001–4019. https://doi.org/10.1029/2003tc001620

Bahlburg, H., & Berndt, J. (2016). Provenance from zircon U-Pb age distributions in crustally contaminated granitoids. *Sedimentary Geology*, *336*, 161–170. https://doi.org/10.1016/j.sedgeo.2015.08.006

Bahlburg, H., Berndt, J., & Gerdes, A. (2016). The ages and tectonic setting of the Faja Eruptiva de la Puna oriental, Ordovician, NW Argentina. *Lithos*, *256–257*, 41–54. https://doi.org/10.1016/j.lithos.2016.03.018

Bahlburg, H., & Hervé, F. (1997). Geodynamic evolution and tectonostratigraphic terranes of northwestern Argentina and northern Chile. *Bulletin of the Geological Society of America*, *109*(7), 869–884. https://doi.org/10.1130/0016-7606(1997)109<0869:geatto>2.3.co;2

Bea, F. (2012). The sources of energy for crustal melting and the geochemistry of heat-producing elements. *Lithos*, *153*, 278–291. https://doi.org/10.1016/j.lithos.2012.01.017

Beaumont, C., Jamieson, R. A., Nguyen, M. H., & Lee, B. (2001). Himalayan tectonics explained by extrusion of a low-viscosity crustal channel coupled to focused surface denudation. *Nature*, *414*(6865), 738–742. https://doi.org/10.1038/414738a

Black, L. P., Kamo, S. L., Allen, C. M., Aleinikoff, J. N., Davis, D. W., Korsch, R. J., & Foudoulis, C. (2003). TEMORA 1: A new zircon standard for Phanerozoic U–Pb geochronology. *Chemical Geology*, *200*(1), 155–170. https://doi.org/10.1016/s0009-2541(03)00165-7

Braun, J., Van Der Beek, P., & Batt, G. (2006). *Quantitative thermochronology: Numerical methods for the interpretation of thermochronological data* (pp. 1–258). Cambridge University Press.

Brown, M. (2010). Melting of the continental crust during orogenesis: The thermal, rheological, and compositional consequences of melt transport from lower to upper continental crust 1.

Brown, M. (2013). Granite: From Genesis to emplacement. *Bulletin of the Geological Society of America*, *125*(7–8), 1079–1113. https://doi.org/10.1130/b30877.1

Büttner, S. H. (2009). The Ordovician Sierras Pampeanas–Puna basin connection: Basement thinning and basin formation in the Proto-Andean back-arc. *Tectonophysics*, *477*(3–4), 278–291. https://doi.org/10.1016/j.tecto.2009.02.003

Büttner, S. H., Glodny, J., Lucassen, F., Wemmer, K., Erdmann, S., Handler, R., & Franz, G. (2005). Ordovician metamorphism and plutonism in the Sierra de Quilmes metamorphic complex: Implications for the tectonic setting of the northern Sierras Pampeanas (NW Argentina). *Lithos*, *83*(1–2), 143–181. https://doi.org/10.1016/j.lithos.2005.01.006

Caddick, M. J., Konopásek, J., & Thompson, A. B. (2010). Preservation of garnet growth zoning and the duration of prograde metamorphism. *Journal of Petrology*, *51*(11), 2327–2347. https://doi.org/10.1093/petrology/egq059

Casquet, C., Alasino, P., Galindo, C., Pankhurst, R., Dahlquist, J., Baldo, E. G., et al. (2021). The Faja Eruptiva of the Eastern Puna and the Sierra de Calalaste, NW Argentina: U–Pb zircon chronology of the early Famatinan orogeny. *Journal of Iberian Geology*, *47*(1), 15–37. https://doi.org/10.1007/s41513-020-00150-z

Casquet, C., Pankhurst, R. J., Rapela, C. W., Galindo, C., Dahlquist, J., Baldo, E., et al. (2005). Grenvillian massif-type anorthosites in the Sierras Pampeanas. *Journal of the Geological Society London*, *162*(1), 9–12. https://doi.org/10.1144/0016-764904-100

Casquet, C., Ramacciotti, C., Larrovere, M. A., Verdecchia, S., Murra, J., Baldo, E. G., et al. (2021). The Rinconada phase: A regional tectono-metamorphic event of Silurian age in the pre-Andean basement of Argentina. *Journal of South American Earth Sciences*, *111*, 103432. https://doi.org/10.1016/j.jsames.2021.103432

Catlos, E. J., Baker, C., Sorensen, S. S., Çemen, I., & Hançer, M. (2010). Geochemistry, geochronology, and cathodoluminescence imagery of the Salihli and Turgutlu granites (central Menderes massif, western Turkey): Implications for Aegean tectonics. *Tectonophysics*, *488*(1–4), 110–130. https://doi.org/10.1016/j.tecto.2009.06.001

Cavalcante, C., Hollanda, M. H., Vauchez, A., & Kawata, M. (2018). How long can the middle crust remain partially molten during orogeny? *Geology*, *46*(10), 839–842. https://doi.org/10.1130/g45126.1

Cawood, P. A. (2005). Terra Australis Orogen: Rodinia breakup and development of the Pacific and Iapetus margins of Gondwana during the Neoproterozoic and Paleozoic. *Earth-Science Reviews*, *69*(3–4), 249–279. https://doi.org/10.1016/j.earscirev.2004.09.001

Cherniak, D. J. (2010). Diffusion in accessory minerals: Zircon, titanite, apatite, monazite and xenotime. *Reviews in Mineralogy and Geochemistry*, *72*(1), 827–869. https://doi.org/10.2138/rmg.2010.72.18

Cherniak, D. J., & Pyle, J. M. (2008). Th diffusion in monazite. *Chemical Geology*, *256*(1–2), 52–61. https://doi.org/10.1016/j.chemgeo.2008.07.024

Cherniak, D. J., & Watson, E. B. (2001). Pb diffusion in zircon. *Chemical Geology*, *172*(1–2), 5–24. https://doi.org/10.1016/s0009-2541(00)00233-3

Cherniak, D. J., Watson, E. B., Grove, M., & Harrison, T. M. (2004). Pb diffusion in monazite: A combined RBS/SIMS study. *Geochimica et Cosmochimica Acta*, *68*(4), 829–840. https://doi.org/10.1016/j.gca.2003.07.012

Coggon, R., & Holland, T. J. B. (2002). Mixing properties of phengitic micas and revised garnet-phengite thermobarometers. *Journal of Metamorphic Geology*, *20*(7), 683–696. https://doi.org/10.1046/j.1525-1314.2002.00395.x

Cristofolini, E. A., Otamendi, J. E., Walker, B. A., Tibaldi, A. M., Armas, P., Bergantz, G. W., & Martino, R. D. (2014). A middle Paleozoic shear zone in the Sierra de Valle Fértil, Argentina: Records of a continent-arc collision in the Famatinian margin of Gondwana. *Journal of South American Earth Sciences*, *56*, 170–185. https://doi.org/10.1016/j.jsames.2014.09.010

Curie, C. A., & Hyndman, R. D. (2006). The thermal structure of subduction zone back arcs. *Journal of Geophysical Research*, *111*(8), B08404. https://doi.org/10.1029/2005jb004024

Dahlquist, J., Verdecchia, S. O., Baldo, E., Basei, M., Alasino, P., Rapela, C. W., et al. (2016). Early Cambrian U-Pb zircon age and Hf-isotope data from the Guasayán pluton, Sierras Pampeanas, Argentina: Implications for the northwestern boundary of the Pampean arc. *Andean Geology*, *1*(43), 137–150. https://doi.org/10.5027/andgeov43n1-a08

Deer, W. A., Howie, R. A., & Zussman, J. (1992). *An introduction to the rock-forming minerals* (2nd ed.). Mineralogical Society of Great Britain and Ireland.

Dodson, M. H. (1973). Closure temperature in cooling geochronological and petrological systems. *Contributions to Mineralogy and Petrology*, *40*(3), 259–274. https://doi.org/10.1007/bf00373790

Ducea, M. N., Bergantz, G. W., Crowley, J. L., & Otamendi, J. (2017). Ultrafast magmatic buildup and diversification to produce continental crust during subduction. *Geology*, *45*(3), 235–238. https://doi.org/10.1130/g38726.1

Ducea, M. N., Otamendi, J. E., Bergantz, G., Stair, K. M., Valencia, V. A., & Gehrels, G. E. (2010). Timing constraints on building an intermediate plutonic arc crustal section: U-Pb zircon geochronology of the Sierra Valle Fértil-La Huerta, Famatinian arc, Argentina. *Tectonics*, *29*(4), TC4002. https://doi.org/10.1029/2009tc002615

Escayola, M. P., van Staal, C. R., & Davis, W. J. (2011). The age and tectonic setting of the Puncoviscana Formation in northwestern Argentina: An accretionary complex related to Early Cambrian closure of the Puncoviscana Ocean and accretion of the Arequipa-Antofalla block. *Journal of South American Earth Sciences*, *32*(4), 438–459. https://doi.org/10.1016/j.jsames.2011.04.013

Faccenda, M., Gerya, T. V., & Chakraborty, S. (2008). Styles of post-subduction collisional orogeny: Influence of convergence velocity, crustal rheology and radiogenic heat production. *Lithos*, *103*(1), 257–287. https://doi.org/10.1016/j.lithos.2007.09.009

Farias, P., Weinberg, R., Sola, A., & Becchio, R. (2020). From crustal thickening to Orogen-parallel escape: The 120-Myr-long HT-LP evolution recorded by Titanite in the Paleozoic Famatinian backarc, NW Argentina. *Tectonics*, *39*(9), e2020TC006184. https://doi.org/10.1029/2020tc006184

Finch, M., Hasalová, P., Weinberg, R. F., & Fanning, C. M. (2014). Switch from thrusting to normal shearing in the Zanskar shear zone, NW Himalaya: Implications for channel flow. *Bulletin of the Geological Society of America*, *126*(7–8), 892–924. https://doi.org/10.1130/b30817.1

Finch, M. A., Weinberg, R. F., Barrote, V. R., & Cawood, P. A. (2021). Hf isotopic ratios in zircon reveal processes of anatexis and pluton construction. *Earth and Planetary Science Letters*, *576*, 117215. https://doi.org/10.1016/j.epsl.2021.117215

Finch, M. A., Weinberg, R. F., Fuentes, M. G., Hasalová, P., & Becchio, R. (2015). One kilometre-thick ultramylonite, Sierra de Quilmes, Sierras Pampeanas, NW Argentina. *Journal of Structural Geology*, *72*, 33–54. https://doi.org/10.1016/j.jsg.2015.01.002

Finch, M. A., Weinberg, R. F., Hasalová, P., Becchio, R., Fuentes, M. G., & Kennedy, A. (2017). Tectono-metamorphic evolution of a convergent back-arc: The Famatinian orogen, Sierra de Quilmes, Sierras Pampeanas, NW Argentina. *Bulletin of the Geological Society of America*, *129*, 1602–1621.

Fossen, H., & Cavalcante, G. C. G. (2017). Shear zones—A review. *Earth-Science Reviews*, *171*, 434–455. https://doi.org/10.1016/j.earscirev.2017.05.002

Foster, G., Gibson, H. D., Parrish, R., Horstwood, M., Fraser, J., & Tindle, A. (2002). Textural, chemical and isotopic insights into the nature and behaviour of metamorphic monazite. *Chemical Geology*, *191*(1–3), 183–207. https://doi.org/10.1016/s0009-2541(02)00156-0

Frost, B. R., Chamberlain, K. R., & Schumacher, J. C. (2001). Sphene (titanite): Phase relations and role as a geochronometer. *Chemical Geology*, *172*(1–2), 131–148. https://doi.org/10.1016/s0009-2541(00)00240-0

Gallien, F., Mogessie, A., Bjerg, E., Delpino, S., de Machuca, B. C., Thöni, M., & Klötzli, U. (2010). Timing and rate of granulite facies metamorphism and cooling from multi-mineral chronology on migmatitic gneisses, Sierras de La Huerta and Valle Fértil, NW Argentina. *Lithos*, *114*(1–2), 229–252. https://doi.org/10.1016/j.lithos.2009.08.011

Gao, X. Y., Zheng, Y. F., Chen, Y. X., & Guo, J. (2012). Geochemical and U-Pb age constraints on the occurrence of polygenetic titanites in UHP metagranite in the Dabie orogen. *Lithos*, *136–139*, 93–108. https://doi.org/10.1016/j.lithos.2011.03.020

Garber, J. M., Hacker, B. R., Kylander-Clark, A. R. C., Stearns, M., & Seward, G. (2017). Controls on trace element Uptake in metamorphic titanite: Implications for petrochronology. *Journal of Petrology*, *58*(6), 1031–1057. https://doi.org/10.1093/petrology/egx046

Gardés, E., Montel, J. M., Seydoux-Guillaume, A. M., & Wirth, R. (2007). Pb diffusion in monazite: New constraints from the experimental study of Pb2 + ⇔ Ca2 + interdiffusion. *Geochimica et Cosmochimica Acta*, *71*(16), 4036–4043. https://doi.org/10.1016/j.gca.2007.06.036

Gasser, D., Jeřábek, P., Faber, C., Stünitz, H., Menegon, L., Corfu, F., et al. (2015). Behaviour of geochronometers and timing of metamorphic reactions during deformation at lower crustal conditions: Phase equilibrium modelling and U-Pb dating of zircon, monazite, rutile and titanite from the Kalak Nappe Complex, northern Norway. *Journal of Metamorphic Geology*, *33*(5), 513–534. https://doi.org/10.1111/jmg.12131

Gehrels, G. (2014). Detrital zircon U-Pb geochronology applied to tectonics. *Annual Review of Earth and Planetary Sciences*, *42*(1), 127–149. https://doi.org/10.1146/annurev-earth-050212-124012

Gordon, S. M., Kirkland, C. L., Reddy, S. M., Blatchford, H. J., Whitney, D. L., Teyssier, C., et al. (2021). Deformation-enhanced recrystallization of titanite drives decoupling between U-Pb and trace elements. *Earth and Planetary Science Letters*, *560*, 116810. https://doi.org/10.1016/j.epsl.2021.116810

Grissom, G. C., Debari, S. M., & Snee, L. W. (1998). Geology of the Sierra de Fiambala, northwestern Argentina: Implications for early Palaeozoic Andean tectonics. *Geological Society, London, Special Publications*, *142*(1), 297–323. https://doi.org/10.1144/gsl.sp.1998.142.01.15

Harlov, D. E., & Hetherington, C. J. (2010). Partial high-grade alteration of monazite using alkali-bearing fluids: Experiment and nature. *American Mineralogist*, *95*(7), 1105–1108. https://doi.org/10.2138/am.2010.3525

Hauser, N., Matteini, M., Omarini, R. H., & Pimentel, M. M. (2011). Combined U–Pb and Lu–Hf isotope data on turbidites of the Paleozoic basement of NW Argentina and petrology of associated igneous rocks: Implications for the tectonic evolution of western Gondwana between 560 and 460 Ma. *Gondwana Research*, *19*(1), 100–127. https://doi.org/10.1016/j.gr.2010.04.002

Hayden, L. A., Watson, E. B., & Wark, D. A. (2008). A thermobarometer for sphene (titanite). *Contributions to Mineralogy and Petrology*, *155*(4), 529–540. https://doi.org/10.1007/s00410-007-0256-y

Hetherington, C. J., Harlov, D. E., & Budzyń, B. (2010). Experimental metasomatism of monazite and xenotime: Mineral stability, REE mobility and fluid composition. *Mineralogy and Petrology*, *99*(3–4), 165–184. https://doi.org/10.1007/s00710-010-0110-1

Holland, T., & Powell, R. (2003). Activity–composition relations for phases in petrological calculations: An asymmetric multicomponent formulation. *Contributions to Mineralogy and Petrology*, *145*(4), 492–501. https://doi.org/10.1007/s00410-003-0464-z

Holland, T. J. B., & Powell, R. (1998). An internally consistent thermodynamic data set for phases of petrological interest. *Journal of Metamorphic Geology*, *16*(3), 309–343. https://doi.org/10.1111/j.1525-1314.1998.00140.x

Hoskin, P. W. O., & Black, L. P. (2000). Metamorphic zircon formation by solid-state recrystallization of protolith igneous zircon. *Journal of Metamorphic Geology*, *18*(4), 423–439. https://doi.org/10.1046/j.1525-1314.2000.00266.x

Hoskin, P. W. O., & Schaltegger, U. (2003). The composition of zircon and igneous and metamorphic petrogenesis. In *Reviews in mineralogy and geochemistry*.

Jackson, S. E., Pearson, N. J., Griffin, W. L., & Belousova, E. A. (2004). The application of laser ablation-inductively coupled plasma-mass spectrometry to in situ U–Pb zircon geochronology. *Chemical Geology*, *211*(1), 47–69. https://doi.org/10.1016/j.chemgeo.2004.06.017

Johnson, T. E., Clark, C., Taylor, R. J. M., Santosh, M., & Collins, A. S. (2015). Prograde and retrograde growth of monazite in migmatites: An example from the Nagercoil Block, southern India. *Geoscience Frontiers*, *6*(3), 373–387. https://doi.org/10.1016/j.gsf.2014.12.003

Kavanagh-Lepage, C., Gervais, F., Larson, K., Graziani, R., & Moukhsil, A. (2023). Deformation induced decoupling between U-Pb and trace elements in titanite revealed through petrochronology and study of localized deformation. *Geoscience Frontiers*, *14*(2), 101496. https://doi.org/10.1016/j.gsf.2022.101496

Kelsey, D. E., Clark, C., & Hand, M. (2008). Thermobarometric modelling of zircon and monazite growth in melt-bearing systems: Examples using model metapelitic and metapsammitic granulites. *Journal of Metamorphic Geology*, *26*(2), 199–212. https://doi.org/10.1111/j.1525-1314.2007.00757.x

Kirkland, C. L., Erickson, T. M., Johnson, T. E., Danišík, M., Evans, N. J., Bourdet, J., & McDonald, B. J. (2016). Discriminating prolonged, episodic or disturbed monazite age spectra: An example from the Kalak Nappe Complex, Arctic Norway. *Chemical Geology*, *424*, 96–110. https://doi.org/10.1016/j.chemgeo.2016.01.009

Kirkland, C. L., Hollis, J., Danišík, M., Petersen, J., Evans, N. J., & McDonald, B. J. (2017). Apatite and titanite from the Karrat Group, Greenland; implications for charting the thermal evolution of crust from the U-Pb geochronology of common Pb bearing phases. *Precambrian Research*, *300*, 107–120. https://doi.org/10.1016/j.precamres.2017.07.033

Kohn, M. J. (2017). Titanite petrochronology. *Reviews in Mineralogy and Geochemistry*, *83*(1), 419–441. https://doi.org/10.2138/rmg.2017.83.13

Kretz, R. (1983). Symbols for rock-forming minerals. *American Mineralogist*, *68*(1–2), 277–279.

Larrovere, M. A., Alasino, P. H., & Baldo, E. G. (2016). The double-vergent ductile shear zone of northwestern sierra de Velasco: Deformation of the middle crust during the Famatinian orogeny. *Revista de la Asociación Geológica Argentina*, *73*(1), 117–133.

Larrovere, M. A., Casquet, C., Aciar, R. H., Baldo, E. G., Alasino, P. H., & Rapela, C. W. (2021). Extending the Pampean orogen in western Argentina: New evidence of Cambrian magmatism and metamorphism within the Ordovician Famatinian belt revealed by new SHRIMP U–Pb ages. *Journal of South American Earth Sciences*, *109*, 103222. https://doi.org/10.1016/j.jsames.2021.103222

Lee, J. K. W., Williams, I. S., & Ellis, D. J. (1997). Pb, U and Th diffusion in natural zircon. *Nature*, *390*(6656), 159–162. https://doi.org/10.1038/36554

Lucassen, F., & Becchio, R. (2003). Timing of high-grade metamorphism: Early Palaeozoic U-Pb formation ages of titanite indicate long-standing high-T conditions at the western margin of Gondwana (Argentina, 26–29°S). *Journal of Metamorphic Geology*, *21*(7), 649–662. https://doi.org/10.1046/j.1525-1314.2003.00471.x

Lucassen, F., Becchio, R., & Franz, G. (2011). The early Palaeozoic high-grade metamorphism at the active continental margin of West Gondwana in the Andes (NW Argentina/N Chile). *International Journal of Earth Sciences*, *100*(2), 445–463. https://doi.org/10.1007/s00531-010-0585-3

Lucassen, F., Becchio, R., Wilke, H. G., Franz, G., Thirlwall, M. F., Viramonte, J., & Wemmer, K. (2000). Proterozoic-Paleozoic development of the basement of the Central Andes (18–26°S)—A mobile belt of the South American craton. *Journal of South American Earth Sciences*, *13*(8), 697–715. https://doi.org/10.1016/s0895-9811(00)00057-2

Mahan, K. H., Goncalves, P., Williams, M. L., & Jercinovic, M. J. (2006). Dating metamorphic reactions and fluid flow: Application to exhumation of high-P granulites in a crustal-scale shear zone, western Canadian Shield. *Journal of Metamorphic Geology*, *24*(3), 193–217. https://doi.org/10.1111/j.1525-1314.2006.00633.x

Mahar, E. M., Baker, J. M., Powell, R., Holland, T. J. B., & Howell, N. (1997). The effect of Mn on mineral stability in metapelites. *Journal of Metamorphic Geology*, *15*(2), 223–238. https://doi.org/10.1111/j.1525-1314.1997.00011.x

Martin, E. L., Collins, W. J., & Spencer, C. J. (2019). Laurentian origin of the Cuyania suspect terrane, western Argentina, confirmed by Hf isotopes in zircon. *Bulletin of the Geological Society of America*, *132*(1–2), 273–290. https://doi.org/10.1130/b35150.1

Martino, R. D. (2003). Ductile deformation shear belts at Pampean ranges near Córdoba, Central Argentina: A review. *Revista de la Asociación Geológica Argentina*, *58*(4), 549–571.

Mattinson, J. M. (1978). Age, origin, and thermal histories of some plutonic rocks from the Salinian block of California. *Contributions to Mineralogy and Petrology*, *67*(3), 233–245. https://doi.org/10.1007/bf00381451

Mezger, K., & Krogstad, E. J. (1997). Interpretation of discordant U-Pb zircon ages: An evaluation. *Journal of Metamorphic Geology*, *15*(1), 127–140. https://doi.org/10.1111/j.1525-1314.1997.00008.x

Miller, H., Adams, C., Aceñolaza, F. G., & Toselli, A. J. (2011). Evolution of exhumation and erosion in western West Gondwanaland as recorded by detrital zircons of late Neoproterozoic and Cambrian sedimentary rocks of NW and Central Argentina. *International Journal of Earth Sciences*, *100*(2), 619–629. https://doi.org/10.1007/s00531-010-0559-5

Mintrone, M., Galli, A., Laurent, O., Chelle-Michou, C., & Schmidt, M. W. (2020). Quantifying frozen melt in crustal rocks: A new melt-o-meter based on zircon rim volumes. *Chemical Geology*, *551*, 119755. https://doi.org/10.1016/j.chemgeo.2020.119755

Montero, P. W., Bea, F., Zinger, T., Scarrow, J. H., Molina, J. F., & Whitehouse, M. J. (2004). 55 million years of continuous anatexis in Central Iberia: Single-zircon dating of the Peña Negra Complex. *Journal of the Geological Society*, *161*(2), 255–263. https://doi.org/10.1144/0016-764903-024

Moser, A. C., Hacker, B. R., Gehrels, G. E., Seward, G. G. E., Kylander-Clark, A. R. C., & Garber, J. M. (2022). Linking titanite U–Pb dates to coupled deformation and dissolution–reprecipitation. *Contributions to Mineralogy and Petrology*, *177*(3), 42. https://doi.org/10.1007/s00410-022-01906-9

Mulcahy, S. R., Roeske, S. M., McClelland, W. C., Ellis, J. R., Jourdan, F., Renne, P. R., et al. (2014). Multiple migmatite events and cooling from granulite facies metamorphism within the Famatina arc margin of northwest Argentina. *Tectonics*, *33*(1), 1–25. https://doi.org/10.1002/2013tc003398

Omarini, R. H., Sureda, R. J., Götze, H. J., Seilacher, A., & Pflüger, F. (1999). Puncoviscana folded belt in northwestern Argentina: Testimony of Late Proterozoic Rodinia fragmentation and pre-Gondwana collisional episodes. *International Journal of Earth Sciences*, *88*(1), 76–97. https://doi.org/10.1007/s005310050247

O'Neill, H. S. C. (2016). The smoothness and shapes of chondrite-normalized rare Earth element patterns in basalts. *Journal of Petrology*, *57*(8), 1463–1508. https://doi.org/10.1093/petrology/egw047

Otamendi, J. E., Castellarini, P. A., Fagiano, M. R., Demichelis, A. H., & Tibaldi, A. M. (2004). Cambrian to Devonian geologic evolution of the Sierra de Comechingones, Eastern Sierras Pampeanas, Argentina: Evidence for the development and exhumation of Continental Crust on the proto-Pacific margin of Gondwana. *Gondwana Research*, *7*(4), 1143–1155. https://doi.org/10.1016/s1342-937x(05)71090-x

Otamendi, J. E., Cristofolini, E. A., Morosini, A., Armas, P., Tibaldi, A. M., & Camilletti, G. C. (2020). The geodynamic history of the Famatinian arc, Argentina: A record of exposed geology over the type section (latitudes 27°–33° south). *Journal of South American Earth Sciences*, *100*, 102558. https://doi.org/10.1016/j.jsames.2020.102558

Pankhurst, R. J., Rapela, C. W., & Fanning, C. M. (2000). Age and origin of coeval TTG, I- and S-type granites in the Famatinian belt of NW Argentina. In *Special paper of the Geological Society of America* (pp. 151–168).

Pankhurst, R. J., Rapela, C. W., Saavedra, J., Baldo, E., Dahlquist, J., Pascua, I., & Fanning, C. M. (1998). The Famatinian magmatic arc in the central Sierras Pampeanas: An early to mid-Ordovician continental arc on the Gondwana margin. *Geological Society, London, Special Publications*, *142*(1), 343–367. https://doi.org/10.1144/gsl.sp.1998.142.01.17

Papapavlou, K., Darling, J. R., Storey, C. D., Lightfoot, P. C., Moser, D. E., & Lasalle, S. (2017). Dating shear zones with plastically deformed titanite: New insights into the orogenic evolution of the Sudbury impact structure (Ontario, Canada). *Precambrian Research*, *291*, 220–235. https://doi.org/10.1016/j.precamres.2017.01.007

Paton, C., Hellstrom, J., Paul, B., Woodhead, J., & Hergt, J. (2011). Iolite: Freeware for the visualisation and processing of mass spectrometric data. *Journal of Analytical Atomic Spectrometry*, *26*(12), 2508–2518. https://doi.org/10.1039/c1ja10172b

Paton, C., Woodhead, J. D., Hellstrom, J. C., Hergt, J. M., Greig, A., & Maas, R. (2010). Improved laser ablation U-Pb zircon geochronology through robust downhole fractionation correction. *Geochemistry, Geophysics, Geosystems*, *11*(3), Q0AA06. https://doi.org/10.1029/2009gc002618

Payne, J. L., Hand, M., Barovich, K. M., & Wade, B. P. (2008). Temporal constraints on the timing of high-grade metamorphism in the northern Gawler Craton: Implications for assembly of the Australian Proterozoic. *Australian Journal of Earth Sciences*, *55*(5), 623–640. https://doi.org/10.1080/08120090801982595

Pouchou, J.-L., & Pichoir, F. (1991). Quantitative analysis of homogeneous or stratified microvolumes applying the model "PAP". In K. F. J. Heinrich & D. E. Newbury (Eds.), *Electron probe quantitation* (pp. 31–75). Springer US.

Powell, R., Holland, T., & Worley, B. (1998). Calculating phase diagrams involving solid solutions via non-linear equations, with examples using THERMOCALC. *Journal of Metamorphic Geology*, *16*(4), 577–588. https://doi.org/10.1111/j.1525-1314.1998.00157.x

Radice, S., Sola, A. M., Maffini, M. N., D'Eramo, F. J., Weinberg, R. F., Pinotti, L. P., et al. (2021). Constraining the timing and evolution of a long-lived tectonic boundary: An example from the early Paleozoic, Argentina. *Journal of South American Earth Sciences*, *107*, 102892. https://doi.org/10.1016/j.jsames.2020.102892

Ramos, V. A., Jordan, T. E., Allmendinger, R. W., Mpodozis, C., Kay, S. M., Cortés, J. M., & Palma, M. (1986). Paleozoic terranes of the central Argentine-Chilean Andes. *Tectonics*, *5*(6), 855–880. https://doi.org/10.1029/tc005i006p00855

Ramos, V. A., Vujovich, G., Martino, R., & Otamendi, J. (2010). Pampia: A large cratonic block missing in the Rodinia supercontinent. *Journal of Geodynamics*, *50*(3–4), 243–255. https://doi.org/10.1016/j.jog.2010.01.019

Rapela, C. W. (1976a). El Basamento Metamorfico de la Region de Cafayate, Provincia de Salta. Aspectos Petrologicos y Geoquimicos. *Revista de la Asociación Geológica Argentina*, *3*(31), 203–222.

Rapela, C. W. (1976b). Las Rocas Granitoides de la Region de Cafayate, Provincia de Salta. Aspectos Petrologicos y Geoquimicos. *Revista de la Asociación Geológica Argentina*, *4*(31), 260–278.

Rapela, C. W., Pankhurst, R. J., Casquet, C., Baldo, E., Saavedra, J., & Galindo, C. (1998a). Early evolution of the Proto-Andean margin of South America. *Geology*, *26*(8), 707. https://doi.org/10.1130/0091-7613(1998)026<0707:eeotpa>2.3.co;2

Rapela, C. W., Pankhurst, R. J., Casquet, C., Baldo, E., Saavedra, J., Galindo, C., & Fanning, C. M. (1998b). The Pampean Orogeny of the southern proto-Andes: Cambrian continental collision in the Sierras de Cordoba. *Geological Society, London, Special Publications*, *142*(1), 181–217. https://doi.org/10.1144/gsl.sp.1998.142.01.10

Rapela, C. W., Pankhurst, R. J., Casquet, C., Dahlquist, J. A., Mark Fanning, C., Baldo, E. G., et al. (2018). A review of the Famatinian Ordovician magmatism in southern South America: Evidence of lithosphere reworking and continental subduction in the early proto-Andean margin of Gondwana. *Earth-Science Reviews*, *187*, 259–285. https://doi.org/10.1016/j.earscirev.2018.10.006

Rapela, C. W., Pankhurst, R. J., Casquet, C., Fanning, C. M., Baldo, E. G., González-Casado, J. M., et al. (2007). The Río de la Plata craton and the assembly of SW Gondwana. *Earth-Science Reviews*, *83*(1–2), 49–82. https://doi.org/10.1016/j.earscirev.2007.03.004

Rapela, C. W., Pankhurst, R. J., Saavedra, J., Galindo, C., & Galindo, C. (1998). Early evolution of the Proto-Andean margin of South America. *Geology*, *26*(8), 707–710. https://doi.org/10.1130/0091-7613(1998)026<0707:eeotpa>2.3.co;2

Rapela, C. W., Verdecchia, S. O., Casquet, C., Pankhurst, R. J., Baldo, E. G., Galindo, C., et al. (2016). Identifying Laurentian and SW Gondwana sources in the Neoproterozoic to early Paleozoic metasedimentary rocks of the Sierras Pampeanas: Paleogeographic and tectonic implications. *Gondwana Research*, *32*, 193–212. https://doi.org/10.1016/j.gr.2015.02.010

R Core, T. (2020). *R: A language and environment for statistical computing rep*. R Foundation for Statistical Computing. Retrieved from https://www.R-project.org/

Regis, D., Cenki-Tok, B., Darling, J., & Engi, M. (2012). Redistribution of REE, Y, Th, and U at high pressure: Allanite-forming reactions in impure meta-quartzites (Sesia Zone, Western Italian Alps). *American Mineralogist*, *97*(2–3), 315–328. https://doi.org/10.2138/am.2012.3832

Richter, M., Nebel-Jacobsen, Y., Nebel, O., Zack, T., Mertz-Kraus, R., Raveggi, M., & Rösel, D. (2019). Assessment of five monazite reference materials for U-Th/Pb dating using laser-ablation ICP-MS. *Geosciences*, *9*(9), 391. https://doi.org/10.3390/geosciences9090391

Rolland, Y., Cox, S., Boullier, A. M., Pennacchioni, G., & Mancktelow, N. (2003). Rare earth and trace element mobility in mid-crustal shear zones: Insights from the Mont Blanc Massif (Western Alps). *Earth and Planetary Science Letters*, *214*(1–2), 203–219. https://doi.org/10.1016/s0012-821x(03)00372-8

Rollinson, H. (1995). *Using geochemical data: Evaluation, presentation, interpretation* (p. 384). Routledge.

Rossi, J., & Toselli, A. (1976). Migmatization y Metamorfismo en el basamento de la Sierra de Quilmes, al Oeste de Colalao del Valle, Tucuman. *Revista de la Asociación Geológica Argentina*, *2*(31), 83–94.

Rubatto, D. (2002). Zircon trace element geochemistry: Partitioning with garnet and the link between U-Pb ages and metamorphism. *Chemical Geology*, *184*(1–2), 123–138. https://doi.org/10.1016/s0009-2541(01)00355-2

Safipour, R., Carrapa, B., DeCelles, P. G., Thomson, S. N., DeCelles, P. G., Ducea, M. N., et al. (2015). Exhumation of the Precordillera and northern Sierras Pampeanas and along-strike correlation of the Andean orogenic front, northwestern Argentina. In P. G. DeCelles, M. N. Ducea, B. Carrapa, & P. A. Kapp (Eds.), *Geodynamics of a Cordilleran orogenic system: The central Andes of Argentina and Northern Chile*. Geological Society of America.

Schiller, D., & Finger, F. (2019). Application of Ti-in-zircon thermometry to granite studies: Problems and possible solutions. *Contributions to Mineralogy and Petrology*, *174*(6), 51. https://doi.org/10.1007/s00410-019-1585-3

Schwartz, J. J., & Gromet, L. P. (2004). Provenance of a late Proterozoic–early Cambrian basin, Sierras de Córdoba, Argentina. *Precambrian Research*, *129*(1–2), 1–21. https://doi.org/10.1016/j.precamres.2003.08.011

Schwartz, J. J., Gromet, L. P., & Miro, R. (2008). Timing and duration of the calc-alkaline arc of the Pampean Orogeny: Implications for the Late Neoproterozoic to Cambrian evolution of Western Gondwana. *The Journal of Geology*, *116*(1), 39–61. https://doi.org/10.1086/524122

Schwartz, J. J., Stowell, H. H., Klepeis, K. A., Tulloch, A. J., Kylander-Clark, A. R. C., Hacker, B. R., & Coble, M. A. (2016). Thermochronology of extensional orogenic collapse in the deep crust of Zealandia. *Geosphere*, *12*(3), 647–677. https://doi.org/10.1130/ges01232.1

Scibiorski, E., Kirkland, C. L., Kemp, A. I. S., Tohver, E., & Evans, N. J. (2019). Trace elements in titanite: A potential tool to constrain polygenetic growth processes and timing. *Chemical Geology*, *509*, 1–19. https://doi.org/10.1016/j.chemgeo.2019.01.006

Scott, D. J., & St-Onge, M. R. (1995). Constraints on Pb closure temperature in titanite based on rocks from the Ungava orogen, Canada: Implications for U-Pb geochronology and P-T-t path determinations. *Geology*, *23*(12), 1123–1126. https://doi.org/10.1130/0091-7613(1995)023<1123:copcti>2.3.co;2

Semenov, I., & Weinberg, R. F. (2017). A major mid-crustal decollement of the Paleozoic convergent margin of western Gondwana: The Guacha Corral shear zone, Argentina. *Journal of Structural Geology*, *103*, 75–99. https://doi.org/10.1016/j.jsg.2017.08.009

Semenov, I., Weinberg, R. F., Taylor, R. J. M., & Jourdan, F. (2019). Prolonged Movement on a >10-km-Wide thrust during early Paleozoic orogens in the Gondwana margin of NW Argentina. *Tectonics*, *38*(8), 3210–3236. https://doi.org/10.1029/2018tc005417

Seydoux-Guillaume, A.-M., Fougerouse, D., Laurent, A. T., Gardés, E., Reddy, S., & Saxey, D. (2019). Nanoscale resetting of the Th/Pb system in an isotopically-closed monazite grain: A combined atom probe and transmission electron microscopy study. *Geoscience Frontiers*, *10*(1), 65–76. https://doi.org/10.1016/j.gsf.2018.09.004

Seydoux-Guillaume, A.-M., Goncalves, P., Wirth, R., & Deutsch, A. (2003). Transmission electron microscope study of polyphase and discordant monazites: Site-specific specimen preparation using the focused ion beam technique. *Geology*, *31*(11), 973–976. https://doi.org/10.1130/g19582.1

Sims, J. P., Ireland, T. R., Camacho, A., Lyons, P., Pieters, P. E., Skirrow, R. G., et al. (1998). U-Pb, Th-Pb and Ar-Ar geochronology from the southern Sierras Pampeanas, Argentina: Implications for the Palaeozoic tectonic evolution of the western Gondwana margin. *Geological Society, London, Special Publications*, *142*(1), 259–281. https://doi.org/10.1144/gsl.sp.1998.142.01.13

Sláma, J., Kosler, J., Condon, D. J., Crowley, J. L., Gerdes, A., Hanchar, J. M., et al. (2008). Plešovice zircon—A new natural reference material for U–Pb and Hf isotopic microanalysis. *Chemical Geology*, *249*(1), 1–35. https://doi.org/10.1016/j.chemgeo.2007.11.005

Sola, A. M., Becchio, R. A., & Pimentel, M. M. (2013). Petrogenesis of migmatites and leucogranites from Sierra de Molinos, Salta, northwest Argentina: A petrologic and geochemical study. *Lithos*, *177*, 470–491. https://doi.org/10.1016/j.lithos.2013.07.025

Sola, A. M., Hasalová, P., Weinberg, R. F., Suzaño, N. O., Becchio, R. A., Hongn, F. D., & Botelho, N. (2017). Low-P melting of metapelitic rocks and the role of H_2O: Insights from phase equilibria modelling. *Journal of Metamorphic Geology*, *35*(9), 1131–1159. https://doi.org/10.1111/jmg.12279

Stearns, M., Hacker, B., Ratschbacher, L., Rutte, D., & Kylander-Clark, A. (2015). Titanite petrochronology of the Pamir gneiss domes: Implications for middle to deep crust exhumation and titanite closure to Pb and Zr diffusion. *Tectonics*, *34*(4), 784–802. https://doi.org/10.1002/2014tc003774

Taylor, R. J. M., Clark, C., Fitzsimons, I. C. W., Santosh, M., Hand, M., Evans, N., & McDonald, B. (2014). Post-peak, fluid-mediated modification of granulite facies zircon and monazite in the Trivandrum Block, southern India. *Contributions to Mineralogy and Petrology*, *168*(2), 1–17. https://doi.org/10.1007/s00410-014-1044-0

Taylor, R. J. M., Kirkland, C. L., & Clark, C. (2016). Accessories after the facts: Constraining the timing, duration and conditions of high-temperature metamorphic processes. *Lithos*, *264*, 239–257. https://doi.org/10.1016/j.lithos.2016.09.004

Teufel, S., & Heinrich, W. (1997). Partial resetting of the U-Pb isotope system in monazite through hydrothermal experiments: An SEM and U-Pb isotope study. *Chemical Geology*, *137*(3–4), 273–281. https://doi.org/10.1016/s0009-2541(96)00161-1

Tholt, A., Mulcahy, S. R., McClelland, W. C., Roeske, S. M., Meira, V. T., Webber, P., et al. (2021). Metamorphism of the Sierra de Maz and implications for the tectonic evolution of the MARA terrane. *Geosphere*, *17*(6), 1786–1806. https://doi.org/10.1130/ges02268.1

Toselli, A., Rossi, J., & Rapela, C. W. (1978). El Basamento Metamorfico de la Sierra de Quilmes, Republica Argentina. *Revista de la Asociación Geológica Argentina*, *33*(2), 105–121.

Turner, J. C. M. (1975). Geología del sector oriental de los Departamentos de Santa Victoria e Iruya, Provincia de Salta. República Argentina: Boletín de la Academia Nacional de Ciencias. *Boletin de la Academia Nacional de Ciencias*, *51*, 11–24.

Vauchez, A., Hollanda, M. H. B. M., Monié, P., Mondou, M., & Egydio-Silva, M. (2019). Slow cooling and crystallization of the roots of the Neoproterozoic Araçuaí hot orogen (SE Brazil): Implications for rheology, strain distribution, and deformation analysis. *Tectonophysics*, *766*, 500–518. https://doi.org/10.1016/j.tecto.2019.05.013

Verdecchia, S. O., Ramacciotti, C. D., Casquet, C., Baldo, E. G., Murra, J. A., & Pankhurst, R. J. (2022). Late Famatinian (440–410 Ma) overprint of Grenvillian metamorphism in Grt-St schists from the Sierra de Maz (Argentina): Phase equilibrium modelling, geochronology, and tectonic significance. *Journal of Metamorphic Geology*, *40*(8), 1–35. https://doi.org/10.1111/jmg.12677

Vermeesch, P. (2018). IsoplotR: A free and open toolbox for geochronology. *Geoscience Frontiers*, *9*(5), 1479–1493. https://doi.org/10.1016/j.gsf.2018.04.001

Watson, E. B., Wark, D. A., & Thomas, J. B. (2006). Crystallization thermometers for zircon and rutile. *Contributions to Mineralogy and Petrology*, *151*(4), 413–433. https://doi.org/10.1007/s00410-006-0068-5

Wawrzenitz, N., Krohe, A., Baziotis, I., Mposkos, E., Kylander-Clark, A., & Romer, R. (2015). LASS U-Th-Pb monazite and rutile geochronology of felsic high-pressure granulites (Rhodope, N Greece): Effects of fluid, deformation and metamorphic reactions in local subsystems. *Lithos*, *232*, 266–285. https://doi.org/10.1016/j.lithos.2015.06.029

Weinberg, R. F., Becchio, R., Farias, P., Suzaño, N., & Sola, A. (2018). Early Paleozoic accretionary orogenies in NW Argentina: Growth of West Gondwana. *Earth-Science Reviews*, *187*, 219–247. https://doi.org/10.1016/j.earscirev.2018.10.001

Weinberg, R. F., Wolfram, L. C., Nebel, O., Hasalová, P., Závada, P., Kylander-Clark, A. R. C., & Becchio, R. (2020). Decoupled U-Pb date and chemical zonation of monazite in migmatites: The case for disturbance of isotopic systematics by coupled dissolution-reprecipitation. *Geochimica et Cosmochimica Acta*, *269*, 398–412. https://doi.org/10.1016/j.gca.2019.10.024

White, R. W., Pomroy, N. E., & Powell, R. (2005). An in situ metatexite–diatexite transition in upper amphibolite facies rocks from Broken Hill, Australia. *Journal of Metamorphic Geology*, *23*(7), 579–602. https://doi.org/10.1111/j.1525-1314.2005.00597.x

White, R. W., Powell, R., & Clarke, G. L. (2002). The interpretation of reaction textures in Fe-rich metapelitic granulites of the Musgrave Block, central Australia: Constraints from mineral equilibria calculations in the system K_2O–FeO–MgO–Al_2O_3–SiO_2–H_2O–TiO_2–Fe_2O_3. *Journal of Metamorphic Geology*, *20*(1), 41–55. https://doi.org/10.1046/j.0263-4929.2001.00349.x

White, R. W., Powell, R., & Holland, T. J. B. (2007). Progress relating to calculation of partial melting equilibria for metapelites. *Journal of Metamorphic Geology*, *25*(5), 511–527. https://doi.org/10.1111/j.1525-1314.2007.00711.x

Whitehouse, M. J., & Platt, J. P. (2003). Dating high-grade metamorphism—Constraints from rare-Earth elements in zircon and garnet. *Contributions to Mineralogy and Petrology*, *145*(1), 61–74. https://doi.org/10.1007/s00410-002-0432-z

Williams, M. L., Jercinovic, M. J., Harlov, D. E., Budzyń, B., & Hetherington, C. J. (2011). Resetting monazite ages during fluid-related alteration. *Chemical Geology*, *283*(3–4), 218–225. https://doi.org/10.1016/j.chemgeo.2011.01.019

Williams, M. L., Jercinovic, M. J., & Hetherington, C. J. (2007). Microprobe monazite geochronology: Understanding geologic processes by integrating composition and chronology. In R. Jeanloz, A. L. Albee, K. C. Burke, & K. H. Freeman (Eds.), *Annual review of earth and planetary Sciences* (pp. 137–175).

Wolfram, L. C., Weinberg, R. F., Hasalová, P., & Becchio, R. (2017). How melt segregation affects granite chemistry: Migmatites from the Sierra de Quilmes, NW Argentina. *Journal of Petrology*, *58*(12), 2339–2364. https://doi.org/10.1093/petrology/egy010

Wolfram, L. C., Weinberg, R. F., Nebel, O., Hamza, K., Hasalová, P., Míková, J., & Becchio, R. (2019). A 60-Myr record of continental back-arc differentiation through cyclic melting. *Nature Geoscience*, *12*(3), 215–219. https://doi.org/10.1038/s41561-019-0298-6

Yakymchuk, C., & Brown, M. (2014). Behaviour of zircon and monazite during crustal melting. *Journal of the Geological Society*, *171*(4), 465–479. https://doi.org/10.1144/jgs2013-115

Yakymchuk, C., Kirkland, C. L., & Clark, C. (2018). Th/U ratios in metamorphic zircon. *Journal of Metamorphic Geology*, *36*(6), 715–737. https://doi.org/10.1111/jmg.12307